Large-eddy simulation of radiation fog: Part 1: Impact of dynamics on microphysics

Marie Mazoyer[1], Christine Lac[1], Odile Thouron[2], Thierry Bergot[1], Valery Masson[1], and Luc Musson-Genon[3]

[1]CNRM (CNRS-Meteo-France), UMR3589, Toulouse, France
[2]CERFACS, Toulouse, France
[3]CEREA, France

Correspondence to: Christine Lac (christine.lac@meteo.fr)

Abstract.

Large Eddy Simulations (LES) of a radiation fog event occurring during the ParisFog experiment ~~have been~~are studied with a view ~~of~~to analy~~z~~sing the impact of the dynamics of the boundary layer on the microphysics. The LES, performed with the Meso-NH model at 5 m resolution horizontally and 1 m vertically, and with a 2-moment microphysical scheme, include~~d~~s the drag effect of a tree~~s~~ barrier and the deposition of droplets on vegetation. The model shows ~~a~~ good agreement with the measurements of the near surface dynamic and thermodynamic parameters~~ as well as the cloud water content~~, but overestimates the cloud droplet ~~sizes~~mass and concentration. The blocking effect of the trees induce~~d~~s elevated fog formation, ~~like in the~~as actually observ~~ation~~ed, and horizontal heterogeneities~~, and~~ during the formation. It also limit~~ed~~s ~~the~~ cooling and ~~the~~ cloud water production. The deposition process ~~was~~is found to exert the most significant impact on the fog prediction~~,~~ as it not only erodes the fog near the surface~~,~~ but also modifies the fog life cycle and induces vertical heterogeneities. ~~The~~A comparison with the 2 m horizontal resolution simulation ~~exhibited~~reveals small differences, meaning that ~~the~~ grid convergence ~~was~~is achieved. Conversely, increasing numerical diffusion through a wind advection operator of lower order ~~led~~leads to an overestimation of the near~~-~~-surface microphysical fields and ha~~d~~s ~~almost~~ a very similar effect ~~than~~to removing ~~the effect of~~ the tree~~s~~ barrier. This study allows us to establish the major dynamical ingredients ~~necessary~~needed to ~~perform correctly~~accurately represent the fog life cycle ~~prediction~~ at very high resolution.

1 Introduction

Despite the long-standing interest in understanding fog processes, uncertainties still exist on the physical mechanisms driving fog variability. Forecasting fog remains a challenge ~~due to~~because of the diversity of mechanisms involved during the fog life cycle and their interactions: local ~~dynamics~~flow, turbulence, radiation, microphysics, aerosols, and surface effects. Several field experiments have been carried out since the 1970~~'~~s ~~that brought~~and have contributed to the important progress made in understanding fog processes~~ understanding~~. ~~Among them the~~Noteworthy works include campaigns ~~from~~at Cardington in the UK (Roach et al., 1976; Price, 2011), Fog-82 in Albany, New York (Meyer et al., 1986), Lille 91 in France (Guedalia and Bergot, 1994), a campaign in the Po Valley in Italy (Fuzzi et al., 1998) and ParisFog in France (Haeffelin et al., 2010). Most of them have naturally included measurements of fog droplet spectra~~,~~ and ~~set~~have reported liquid water contents (LWC) in the range of $0.01 - 0.4\,\mathrm{g\,m^{-3}}$ and droplet number concentration (N_c) of a few tens to a hundred per ~~$\mathrm{cm^{-3}}$~~$\mathrm{cm^{3}}$. ~~Hence~~ Roach et al. (1976) ~~related~~reported values of LWC between 0.05 and $0.22\,\mathrm{g\,m^{-3}}$ and N_c between 30 and $100\,\mathrm{cm^{-3}}$ for winter fog cases at Cardington. More recently, Mazoyer et al. (2016) reported N_c ~~for radiation fog~~of less than $150\,\mathrm{cm^{-3}}$ for radiation fog over 3 winters during ParisFog.

Many important features of fog have also been characterized using one-dimensional (1D) modelling (Bergot et al. (2007), Tardif (2007), Stolaki et al. (2015) among others). ~~But~~However, to study some aspects of the characteristics of a fog layer, it has become necessary to explicitly simulat~~ing~~e turbulence motions in ~~a~~ 3D ~~manner has become necessary to improve our understanding of the physical mechanisms involved in a fog layer, since~~as shown by Nakanishi (2000) who was the first to use a large-eddy simulation (LES) for fog. LES is a turbulence modelling technique in which most of the energy-containing eddies are explicitly resolved while eddies smaller than a certain cutoff ~~scale~~size, usually taken equal to the grid spacing, are parametrized by ~~the~~a turbulence scheme. Since then, Porson et al. (2011) have explored the static stability in a fog layer, and Bergot (2013) have show~~ed~~n the various organized structures occurring in a fog layer, which cannot be resolved in 1D. Thanks to these studies, the dynamical characteristics of ~~the~~ radiation fog are more clearly identified during the three stages of the fog life cycle defined by Nakanishi (2000): the onset, ~~the~~ development and ~~the~~ dissipation phases. During the formation phase, small ~~stripes~~banded structures, identified by Bergot (2013) as Kelvin-Helmotz (KH) billows, occur in the middle of the fog layer on dynamical and thermodynamical fields~~, identified by Bergot(2013) as Kelvin-Helmotz (KH) billows,~~. They are sometimes associated ~~to~~with a burst of turbulent kinetic energy (TKE) (Nakanishi (2000) and Bergot (2013)) but this is not always the case (Porson et al. (2011)). During the development phase, the main dynamical processes ~~move~~relocate to the top of the fog layer and are associated ~~to~~with the maximum of TKE and horizontal rolls (Bergot, 2013). During the dissipation phase, coupled processes between the ground and the top of the fog layer explain the spatial variability of fog (Bergot (2015b))~~. B~~ but the link between dynamics and microphysics has not been explored specifically in these LES studies.

The quality of the LES depends on the horizontal and vertical resolutions. ~~Hence~~Beare and MacVean (2004) demonstrated that simulations in stable conditions converge at 2-m horizontal resolution. Very high vertical resolution is also essential to capture the divergence of the radiative fluxes in the first few metres above the surface and therefore to produce ~~a~~the radiative cooling necessary ~~to~~for the formation of fog (Duynkerke, 1999; Tardif, 2007).

So far, most ~~of~~ fog LES studies have considered homogeneous canopies. Only Bergot et al. (2015a) ~~took into~~have taken account of the effect of surface heterogeneities as buildings on radiation fog. Other studies, such as those by Zaïdi et al.(2013) or Dupont and Brunet (2008), have considered the impact of forests on turbulence structures~~, like Zaïdi et al.(2013) or Dupont and Brunet (2008)~~ but not for fog situations. In this study, we will explore a LES of a fog case that was observed during ParisFog and strongly influenced by trees.

Also, very few fog LES studies are based on sophisticated 2-moment microphysical schemes~~,~~ allowing ~~to represent~~ the impact of aerosols ~~impact~~ on the radiation fog life cycle to be represented. Maalick et al. (2016) studied the effects of aerosols on ~~the~~ radiation fog with an LES~~,~~ but in a 2D configuration that could present some limitations for the dynamical patterns of the fog layer. Additionally, most of the studies ~~, with~~using one- or two~~-~~-moment microphysical schemes~~,~~ fail to reproduce realistic liquid water contents ~~(LWC)~~ as they tend to overestimate ~~it~~values near the ground. For instance, Zhang et al. (2014b) simulated $N_c = 800\ \mathrm{cm^{-3}}$ and $LWC = 0.4\ \mathrm{g\,m^{-3}}$ and Stolaki et al. (2015) simulated $N_c = 250\ \mathrm{cm^{-3}}$ and $LWC = 0.34\ \mathrm{g\,m^{-3}}$ near the surface, both in 1D configuration~~,~~. These values ~~that~~ are outside ~~of~~ the range ~~according to~~found by Mazoyer et al. (2016) considering the same site. So ~~one~~the question ~~is: is there a~~of a possible missing mechanism ~~missing~~arises, the inclusion of which might improve the modelling of microphysical fields~~?~~. Considering deposition, the interactions with the ground surface should be an important factor as already shown by Price and Clark (2014) on measurements and von Glasow and Bott (1999) or Zhang et al. (2014b) on 1D simulations.

The goal of this study is to better understand the physical processes dominating the fog life cycle ~~on~~at a complex site and impacting the microphysical fields. LES modelling at very high resolution (1 m vertically and 5 m horizontally) is used with surface heterogeneities (barrier of trees) and a 2-moment microphysical scheme. ~~Sensitivity tests will help to understand the influence of some dynamical processes on the fog life cycle with a focus on microphysical properties.~~In order to establish the main ingredients driving the fog life cycle and the microphysical fields, and to evaluate how dynamics affects the evolution of fog, sensitivity experiments are conducted with the model considered as a laboratory. To our knowledge, this is the first time that an LES study of radiation fog has been performed at such high resolution with a sophisticated microphysic~~s~~al parameterization scheme ~~taking into account~~while considering the effect of heterogeneities such as forests on the fog dynamics and microphysics. In a second article, the impact of aerosol activation on microphysical fields will be explored specifically, allowing ~~to characterize~~ the contribution of the different microphysical processes to be characterized.

Section 2 presents the measurement set-up and the observed case, and describes the numerical model. The reference simulation is analy~~z~~sed in Section 3, and Section 4 is devoted to sensitivity tests. Finally, some conclusions are drawn and perspectives suggested in Section 5.

2 Experimental design and model description

2.1 Measurements set-up

The selected fog event ~~has been~~was observed on 15 November 2011 during the ParisFog field campaign in the winter of 2011-2012 ~~of the ParisFog field campaign~~ (Haeffelin et al., 2010) at the Sirta (Site Instrumental de Recherche par Télédétection Atmosphérique) observatory (48.713 °N and 2.208 °E). The objective of the ParisFog campaign during three winters from 2010 to 2013 was to better understand the radiative, thermodynamic, dynamic and microphysical processes occurring during the fog life cycle. The site where the instrument platform ~~is~~was installed ~~is~~was a semi-urban area of a complex terrain including forest, lake, meadows and shrubs next to a~~n urban agglomeration~~ built up area. As shown ~~o~~in Figure 1a, the instrumented zone ~~is~~was located near a forest area. Zaïdi et al. (2013) demonstrated the impact of the tree~~s~~ barrier on the observed flow when the wind ~~flows~~was blowing from this ~~side~~direction, ~~just as in~~and our case study was in this configuration. The fog case has already been studied by Stolaki et al. (2015) in ~~the~~a 1D configuration~~, and the reader should refer to this study for the description of the instrumental set-up~~.

~~At the surface, t~~Temperature and humidity sensors were located at heights between 1 and 30 m ~~height~~ on an instrumented mast, with 0.2 K uncertainty ~~for~~on temperature and 2% ~~for~~on relative humidity. Wind speed was measured by two ultrasonic anemometers at 10 m and 30 m above ground level (agl) on the same meteorological mast. Radiative fluxes were measured on a building roof at a height of 10 m ~~height~~ with $5\,\mathrm{W\,m^{-2}}$ and $4\,\mathrm{W\,m^{-2}}$ uncertainties for downward and upward fluxes respectively. Two diffusometers were operated at 3 m and 18 m to provide information on the vertical visibility with an uncertainty of up to 25%. Additionally, radiosondes were launched by Météo-France twice a day ~~in~~from Trappes (48.7°N, 2 °E), ~~localized~~situated 15 km to the ~~North-West~~northwest of Sirta.

~~M~~The microphysical instrumentation ~~was~~has been presented in detail by Mazoyer et al. (2016). A Fog-Monitor 100 (FM-100) provided ~~particles~~the size distribution for particles~~from~~ $2\ \mu\mathrm{m}$ to $50\ \mu m$ in diameter, ~~while~~and the ~~WELAS-2000 provided~~ particle diameter distribution was provided between 0.96 and $10\ \mu\mathrm{m}$ by a WELAS-2000 system. ~~according to Mazoyer et al.(2016).~~ Aerosol particles measurements were performed ~~by~~using a Scanning Mobility Particle Sizer (SMPS) measuring dry aerosol diameters between 10.6 and 496 nm every 5 min, and by a CCN chamber ~~providing~~that gave the CCN number concentration at different supersaturations from 0.1 to 0.5% (Roberts and Nenes, 2005). A RPG-HATPRO water vapour and oxygen multi-channel microwave profiler ~~provided~~was used to measure the Liquid Water Path (LWP) ~~measurements~~ with an error of up to $20\ \mathrm{g\,m^{-2}}$ according to Lohnert and Crewell (2003). We ~~do not have~~did not take measurements of dewfall and fog-droplet deposition.

2.2 Presentation of the observed case

2.2.1 Dynamics and thermodynamics

The radiative fog formed at 0200 UTC on 15 November 2011 and dissipated at the ground around 1000 UTC on the following morning. ~~Favored c~~Conditions ~~of~~favouring fog were due to a ridge at 500 hPa centred over the North Sea and anticyclonic conditions near the surface. One of the features of this event ~~is~~was that it ~~is an~~concerned elevated fog~~ event~~, formed by a cloud layer 150 m agl and followed ~~shortly~~30 min later by fog at the surface. As underlined by Stolaki et al. (2015), this characteristic is very common at Sirta ~~since~~and 88% of the radiation fog events ~~formed~~ during the field experiment were also elevated~~, but~~. However, they were not classified as stratus lowering~~,~~ as they were followed rapidly by formation of fog at the surface. A delay of 30 min between the formation at 150 m height and at the ground seems too short to be a stratus lowering, which is mainly driven by the evaporation of slowly falling droplets that cool the sub-cloud layer (Dupont et al., 2012). This suggests that this ~~property~~type of radiation fog could be linked with, and specific to, the configuration of the Sirta site.

The fog case is presented ~~according to~~following the three phases of the fog life cycle defined by Nakanishi (2000). Before the fog onset, between 2200 and 0200 UTC, the surface boundary layer was stable and a near-surface cooling was observed, ~~as well as a moistening~~inducing an increase in relative humidity (Fig. 2). Between 0000 and 0130 UTC, the relative humidity (RH) near the ground remained nearly constant around 97%. Wind ~~speed~~ at 10 m height was light (speed around $1.8\ \mathrm{m\,s^{-1}}$) as ~~well as~~was TKE, with small variability (Fig. 3). At 0200 UTC, the attenuated backscatter coefficient of the lidar increased significantly at 150 m agl (not shown), revealing the formation of liquid water at this height, while the RH at the surface remained at 97%. Then the cloud base height progressively subsided during about 30 min, until it reached the ground, while the near-surface temperature continued to decrease by about $1\ K$. At 0230 UTC, the apparition of fog at the ground was associated ~~to~~with a temperature ~~convergence~~homogenization in the first 30 metres, ~~as described in~~called temperature convergence by Price (2011)~~,~~ and corresponding to a neutral layer. The downwelling longwave (LWD) radiation flux increased progressively ~~up~~ to $325\ \mathrm{W\,m^{-2}}$ during the development of the fog layer (Fig. 4).

Then, during the fog development and mature phases, between 0200 and 0700 UTC, the near-surface layer remained quasi-neutral and temperature at the different levels remained constant. The 10 m wind speed presented a higher temporal variability than previously, as ~~well as~~did the TKE. Around 0400 UTC, the TKE at 10 m height increased significantly, by $0.5\ \mathrm{m^2\,s^{-2}}$, and ~~remained then constant~~then presented some variability around this value, while maintaining a positive vertical gradient ~~of TKE. According to Stolaki et al.(2015) and Dabas et al.(2012), t~~ . The sodar indicated that the fog top height reached a maximum height of 300 m agl during ~~its~~the mature phase (Stolaki et al.(2015), Dabas et al.(2012)).

At the beginning of the dissipation phase, from 0700 UTC, the surface temperature increased slowly (less than 0.5 K in 2 hours) and then more significantly after 0900 UTC. At 1000 UTC, the downward SW fluxes exceeded $100\ \mathrm{W\,m^{-2}}$, while near-surface temperature had increased by 1 K compared to the pre-sunrise values. 30 m TKE decreased from 0800 UTC to 1000 UTC, while 10 m TKE remained approximately constant.

2.2.2 Microphysics

Measurements of ~~liquid droplet~~ microphysics near the surface indicated a sharp increase ~~of LWC~~in cloud mixing ratio (r_c) and droplet concentration (N_c) at the fog onset just after 02~~0~~30 UTC (Fig. 5 in solid lines), ~~up to~~reaching $N_c = 53\ \mathrm{cm^{-3}}$ and ~~$LWC = 0.035\ \mathrm{g\,m^{-3}}$~~$r_c = 0.02\ \mathrm{g\,kg^{-1}}$. ~~They~~This corresponded to a drop ~~of~~in the near-surface visibility from 5000 m to less than 500 m (Fig. 6a in black line). The initial elevated structure of the fog ~~leaded to~~led to an earlier decrease of the visibility at 18 m than at 3 m agl, with a time lag of the order of 30 min. Until 0730 UTC, ~~LWC~~r_c and N_c decreased ~~then~~ slowly, ~~while~~inducing a small increase of the visibility at 3 m and 18 m (not shown)~~ remained almost constant~~. Between 0730 and 0800 UTC, ~~LWC~~cloud mixing ratio and droplet concentration at 3 m decreased strongly, allowing ~~an increase of~~ the visibility at 3 m ~~up~~to increase to 2000 m. At 18 m agl, the visibility remained ~~smaller~~less than 1300 m. ~~But t~~The fog at the surface reformed just after 0800 UTC, reaching $N_c = 30\ cm^{-3}$ and ~~$LWC = 0.024\ \mathrm{g\,m^{-3}}$~~$r_c = 0.02\ \mathrm{g\,kg^{-1}}$, ~~and~~with a visibility of less than 500 m, before definitively dissipating at 1000 UTC. The particle size distribution (PSD) indicated that 95% of the droplets ~~with~~had a diameter of less than 20 μm, meaning that there ~~is~~was probably a very small impact of the coalescence process. Sampled at 3 stages of the event, ~~it~~the PSD evolved during the fog life cycle and appeared consistent with the classification of Wendisch et al. (1998) (Fig. 5d). The “initial phase”(in red, at 0250 UTC) was characterized by a small droplet size~~,~~ but ~~already~~ a second mode between 8 and 12 $\mu\mathrm{m}$ was already visible, ~~that~~which persisted ~~during~~through the 3 stages. During the mature phase (in blue, at 0500 UTC), also called the “mass transfer stage”, larger droplets ~~are numerous~~, up to 22 $\mu\mathrm{m}$, were numerous. During the dissipation phase (in green, at 0700 UTC), the concentration of larger droplets fell but remained higher than initially~~the spectrum was between the two previous ones with a reduction of the largest droplets~~. Hence the spectral shape remained bimodal during the fog life cycle.

The maximum ~~of~~ LWP measured by the profiler was reached around 0730 UTC, at the beginning of the fog dissipation phase, with 70 $\mathrm{g\,m^{-2}}$ (Fig. 5c). The non-zero values (5 $\mathrm{g\,m^{-2}}$) before the fog onset are ~~included in~~within the error range of the measurement.

2.3 Model description

2.3.1 Presentation of the model

The non-hydrostatic anelastic research model Meso-NH (Lafore et al., 1998) (see http://mesonh.aero.obs-mip.fr) ~~was~~is used here in a LES configuration. The LES ~~was~~is based on a 3D turbulent scheme with a prognostic turbulent kinetic energy (TKE) (Cuxart et al., 2000) and a Deardorff mixing length (Deardorff, 1980).

The atmospheric model ~~was~~is coupled with the ISBA surface scheme (Interaction between Soil Biosphere and Atmosphere, Noilhan and Planton (1989)) through the SURFEX model (Masson et al., 2013). This scheme simulates the exchanges of energy and water between the land surface (soil, vegetation and snow) and the atmosphere above it. It uses five prognostic equations for deep temperature, deep soil water content, surface temperature, surface soil water content and water interception storage by vegetation.

In order to ~~take into account~~consider the impact of trees ~~on~~at the instrument~~al~~ed site, we used the drag approach developed by Aumond et al. (2013) for a vegetation canopy. ~~Indeed, Aumond et al.(2013)~~ These authors and Zaïdi et al. (2013) have shown ~~the best results of~~that the drag approach ~~compared to~~gives better results than the classical roughness law ~~to~~when reproduc~~e~~ing the turbulence downstream of a forest area. ~~It~~The drag approach consists of introducing an additional term into the momentum and TKE equations as follows:

$$\frac{\partial \alpha}{\partial t}_{DRAG} = -C_d A_f(z)\alpha\sqrt{u^2+v^2} \tag{1}$$

where α represents u and v horizontal wind components and TKE, C_d is the drag coefficient, set ~~as~~to 0.2, and $A_f(z)$ is the canopy area density, representing the surface area of the trees facing the flow per unit volume of canopy. ~~It is a combination of~~$A_f(z)$ is the product of the fraction of vegetation in the grid cell by the leaf area index (LAI) and by a weighting function ~~that~~ represent~~s~~ing the shape of the trees~~. The vertical profile is~~, as presented in Aumond et al. (2013). The trees introduced in the simulation domain for the land surface scheme correspond to~~We have considered a~~ Atlantic coast broad leaved trees.

For the microphysics, the model include~~d~~s a two-moment bulk warm microphysical scheme (Khairoutdinov and Kogan, 2000; Geoffroy et al., 2008), that considers droplet concentration N_c and mixing ratio r_c as prognostic variables for the fog. An additional prognostic variable N_{ccn} is used to account for already activated CCN, following the activation scheme of Cohard et al. (2000c). The aerosols are assumed to be lognormally distributed and the activation spectrum is prescribed as:

$$N_{ccn} = C{S_{max}}^k F(\mu, k/2, k/2+1, -\beta {S_{max}}^2) \tag{2}$$

where N_{ccn} is the concentration of activated aerosol, $F(a,b;c;x)$ is the hypergeometric function, C (m^{-3}) is the concentration of aerosols, and k,μ and β are adjustable shape parameters associated with the characteristics of the aerosol size spectrum such as the geometric mean radius ($\bar{r}$) and the geometric standard deviation (σ), as well as solubility of the aerosols (ε_m) and temperature (T) (see below for the values ~~for~~in our case study). S_{max} is the maximum of supersaturation, verifying $\frac{dS}{dt} = 0$. The evolution of the supersaturation S includes three terms accounting~~respectively~~ the effects of a convective ascent ~~using~~of vertical velocity w, the growth of droplets by condensation for the newly activated droplets, and a radiative cooling, as in Zhang et al. (2014b):

$$\frac{dS}{dt} = \phi_1 w - \phi_2 \frac{dr_c}{dt} + \phi_3 \frac{dT}{dt}|_{RAD} \tag{3}$$

where $\phi_1(T)$, $\phi_2(T,P)$ and $\phi_3(T)$ are functions of temperature and pressure. Following Pruppacher et al. (1998) and after simplification, S_{max} can be diagnosed by:

$$S_{max}{}^{k+2}.F(\mu, k/2, k/2+1, -\beta S_{max}{}^2) = \frac{\left(\phi_1 w + \phi_3 \frac{dT}{dt}|_{RAD}\right)^{3/2}}{2kc\pi\rho_w \phi_2{}^{3/2} B(k/2, 3/2)} \tag{4}$$

with B the Beta function and ρ_w the density of water. Thus, the aerosols activated are exactly those with a critical supersaturation lower than S_{max}. The number of aerosols really activated is then the difference between the number of activable aerosols and the number of aerosols previously activated during the simulation.

The condensation/evaporation rate is derived using the Langlois (1973) saturation adjustment scheme. The cloud droplet sedimentation, that is the gravitational settlement of droplets, is computed by considering a Stokes law for the cloud droplet sedimentation velocity and ~~by~~ assuming that the cloud droplet size distribution $n_c(D)$ fits a generalized Gamma law:

$$n_c(D) = N_c \frac{\alpha}{\Gamma(\nu)} \lambda^{\alpha\nu} D^{\alpha\nu - 1} exp(-(\lambda D)^{\alpha}) \tag{5}$$

where λ is the slope parameter, depending on the prognostic variables r_c and N_c:

$$\lambda = \left(\frac{\pi}{6}\rho_w \frac{\Gamma(\nu + 3/\alpha)}{\Gamma(\nu)} \frac{N_c}{\rho_a r_c}\right)^{1/3} \tag{6}$$

α and ν are the parameters of the Gamma law, and ρ_a is the density of dry air. They were adjusted using droplet spectra measurements from the FM-100 database of our case study and were set at $\alpha = 1$ and $\nu = 8$. These parameters are also used for the radiative transfer.

In addition to droplet sedimentation, fog deposition is also introduced which represents direct droplet interception by the plant canopies. In ~~nature~~the real world, it results from turbulent exchange of fog water between the air and the surface underneath, leading to collection (Lovett et al., 1997). In numerical weather prediction models (NWP), this process is most of the time not included, such as in the French NWP model AROME (Seity et al., 2011) whose physics comes from Meso-NH. As a new process to introduce, only a simple formulation of the deposition process is considered here as a first step, in order to perform a sensitivity study. ~~Here, t~~ The fog deposition flux F_{DEP} is predicted at the first level of the atmospheric model (50 cm height) for grassy areas, and over the 15 m height for trees, in a simplistic way following Zhang et al. (2014b): $F_{DEP} = \rho_a \chi V_{DEP}$ with $\chi = r_c, N_c$ and where V_{DEP} is the deposition velocity. In a review based on measurements and parametrizations, Katata (2014) showed that V_{DEP} values ranged from 2.1 to $8.0\,\mathrm{cm\,s^{-1}}$ for short vegetation. ~~A more complete~~

~~approach would be to include a dependance of V_{DEP} with momentum transport and also with LAI, but we supposed h~~Here ~~that~~ V_{DEP} is assumed to be constant, equal to $2\ \mathrm{cm\,s^{-1}}$. A test of sensitivity ~~test~~ to this value ~~will be~~is presented below. Water sedimentation and deposition amounts are ~~supplied~~input to the humidity storage of the surface model. A more complete approach in a further study would include a dependance of V_{DEP} on momentum transport as in von Glasow and Bott (1999) and also on LAI.

The radiative transfer ~~was~~is computed with the ECMWF radiation code, using the Rapid Radiation Transfer Model (RRTM, Mlawer et al. (1997)) for longwave and Morcrette (1991) for shortwave radiation~~s~~. Cloud optical properties for LW and SW radiation ~~took~~take ~~into~~ account of the cloud droplet concentration in addition to the cloud mixing ratio. For SW radiation, the effective radius of cloud particle is calculated from the 2-moment microphysical scheme, the optical thickness is parametrized according to Savijärvi et al. (1997), the asymetry factor from Fouquart et al. (1991) and the single scaterring albedo from Slingo (1989). For LW radiation, cloud water optical properties refer to Savijärvi et al. (1997).

2.3.2 Diagnostics of visibility

Visibility can be diagnosed assuming an exponential scattering law:

$$VIS = -\frac{ln\varepsilon}{\beta} \tag{7}$$

with β the extinction coefficient, and using a visual range defined by a liminal contrast ε of 0.02 (Koschmeider, 1924). The most common parametrizations used to diagnose the visibility with droplet properties in models ~~with~~employing 1-moment microphysical schemes are expressed as:

$$VIS = \frac{a}{(\rho_a r_c)^b} \tag{8}$$

where a is 0.027 and b is 0.88 for Kunkel (1984) (units of r_c and VIS are $\mathrm{g\,kg^{-1}}$ and km respectively).

When droplet concen~~cen~~tration N_c is taken into account with 2-moment microphysical schemes, the diagnostic becomes:

$$VIS = \frac{c}{(\rho_a r_c N_c)^d} \tag{9}$$

where c is 1.002 and d is 0.6473 for Gultepe et al. (2006) ~~developed with eastern Canada~~based on observations made in eastern Canada, and c is 0.187 and d is 0.34 for Zhang et al. (2014a) from measurements made in the polluted North China Plain ~~measurements~~.

Measurements of visibility can be employed to estimate the validity of the visibility diagnostics the most often used ~~for~~by models. Hence, the three formulations were applied to the observed ~~LWC~~r_c and N_c and compared to the observed visibility in order to determine which one fit~~s~~ted ~~the best~~ the observed values best (Fig. 6a). In our case study, Zhang et al. (2014a)'s parametrization was the most adapted to the observations ~~of our case study~~, as it is more sensitive to low ~~LWC~~r_c and N_c values, even ~~if~~though it tended to underestimate ~~slightly~~ the observed visibility slightly. Diagnostics from Kunkel (1984), and even more so from Gultepe et al. (2006) ~~even more~~, markedly ~~under~~overestimated the 3 m observed visibility ~~in our case study~~.

2.3.3 Simulation set-up

For the reference simulation (noted REF), the horizontal resolution ~~wa~~is 5 m over a domain size of 200 x 200 grid points. 126 vertical levels ~~we~~are used between the soil and the top of the model at 1500 m. The vertical resolution ~~wa~~is 1 m for the first 50 m and increased~~s then~~ slightly above this height. Momentum ~~variables were transported~~is advected with a fourth-order centred scheme (noted CEN4TH), whereas scalar variables ~~we~~are ~~transported~~advected with the PPM (Piecewise Parabolic Method) scheme (Colella and Woodward, 1984). The time step ~~wa~~is 0.1 s. The domain of simulation is presented ~~on~~in Figure 1b, with a tree~~s~~ barrier ~~of~~ 15 m ~~height~~high and 100 m wide perpendicular to the wind direction. The rest of the domain ~~wa~~is composed of grass. The lateral boundary conditions ~~we~~are cyclic. The radiation scheme ~~wa~~is called every second.

The simulation began at 2320 UTC on 14 November 2011 before the fog formation, and covered 12 h. Temperature, humidity and wind speed vertical profiles were initialized with data from the radiosonde launched ~~in~~from Trappes. Meteorological conditions at Trappes can differ slightly from those at the Sirta site. Therefore wind, temperature and humidity were modified in the nocturnal boundary layer up to 400 m agl to ~~adjust with~~fit the data recorded at the 30 m meteorological mast at the Sirta site, as illustrated ~~on~~in Fig. A.1. The soil temperature and ~~moistening~~moisture ~~we~~are given by the soil measurements, corresponding to a surface temperature of 276 K and a soil moisture of 70%. Following the profiles from soundings, a geostrophic wind of $8\,m\,s^{-1}$ was prescribed ~~as a forcing~~, without any other forcing. To generate turbulence ~~in addition to the effect of trees~~, a white noise of 0.5 K was applied in the first 100 m in addition to the effect of trees.

It was also necessary to characterize the aerosol size spectrum for Eq.2. The supersaturations reached in fog were lower than 0.1% meaning that the CCNC measurements were not directly usable, as shown by Hammer et al. (2014) and Mazoyer et al. (2016). ~~But~~However, when using the Kappa-Köhler theory and the SMPS observations, the aerosols concentration at supersaturations under 0.1% can be retrieved ~~knowing~~if the aerosol hygroscopicity (κ) at these supersaturations is known. This method, proposed by Mazoyer et al. (2016), ~~has been~~was applied to our case study in the hour before the fog onset. The activation spectrum was thus computed from observations above 0.1% supersaturation, and from computation ~~under~~below 0.1%. ~~A fit of t~~This computed activation spectrum ~~wa~~is ~~applied~~fitted according to Eq.2 (Fig. A.2a), corresponding to the size distribution of aerosol~~s~~ particles ~~distribution~~ ($C = 2017$ cm^{-3}, $\sigma = 0.424$, $\bar{r} = 0,1$,$\varepsilon_m = 1$) in red ~~on~~in Fig. A.2b. This does not match the measured distribution (in black) ~~n~~or the lognormal fitted on the accumulation mode (in blue), ~~due to the fact that~~because Cohard et al. (2000c) formulation ~~h~~was not ~~been~~ developed for fog with low supersaturation. ~~Nevertheless, considering that the activation spectrum was deduced from measurements, it includes a good degree of confidence.~~Deducing the activation spectrum from measurements provides the exact solution.

The reference simulation will ~~be~~ now be presented.

3 The reference simulation

The performance of the REF simulation ~~is~~will be first examined, based on a comparison with observed values of thermohygrometric, dynamic, radiative and microphysical parameters near the ground. Considering that the REF simulation reached~~s a~~ good ~~degree of confidence~~agreement with observation, the vertical evolution and horizontal variability of the simulated fog ~~are~~will be then characterized during the different phases of the fog life cycle. It should be emphasized that observations localized at one point ~~were~~will be compared to ~~averaged~~ simulated fields averaged over a~~n~~ horizontal area located downstream of the tree~~s~~ barrier (blue contour area of Fig. 1b) representative of the instrument~~al~~ed area~~, as w~~. We will indeed see that ~~there were significant horizontal heterogeneities over this area~~the simulation domain is divided into 4 parts with significant differences between them, but similar characteristics inside each one.

3.1 Parameters near the surface

3.1.1 Dynamics and thermodynamics

Figure 2 shows the time series of near~~-~~-surface observed and simulated temperature and RH. At the initialization of the simulation, near~~-~~-surface temperatures ~~we~~are in agreement with the observations while RH ~~were~~is very slightly underestimated. During the cooling before ~~the~~ fog onset, the model develop~~ed~~s a ~~too stable~~ layer that is too stable, especially in the ~~5~~ first 5 metres between 0000 and 0100 UTC. The convergence of temperature ~~wa~~is simulated with 30~~-40~~ min~~utes of~~ delay compared to the observations

Considering RH near the surface (and the microphysical fields below), the fog start~~ed~~s to appear around 02~~3~~00 UTC. Between 0430 and ~~0830~~0900 UTC, simulated and observed temperature ~~we~~are in fairly good agreement, with a quasi-neutral near~~-~~-surface layer. The fog start~~ed~~s to dissipate from the ground at ~~0830~~0900 UTC, ~~with~~ approximately one hour ~~and a half~~ ahead of the local observation. This time ~~lag~~discrepancy induce~~d~~s a slight overestimation of near~~-~~-surface temperature, ~~increasing up to~~which is less than 0.5 K at 1100 UTC. ~~But~~Nevertheless, the negative temperature gradient near the surface representative of the development of the convective boundary layer ~~wa~~is quite well reproduced after the beginning of the dissipation.

Dynamical fields at 10 m and 30 m ~~we~~are fairly well reproduced by the model (Fig. 3 in red): the 10 m wind speed (Fig. 3a) ~~wa~~is in good agreement with ~~the~~ observation ~~during all~~throughout the simulation. Until 0300 UTC, a quasi linear increase of TKE ~~wa~~is produced by the model with a higher TKE at 10 m agl ~~higher~~ than at 30 m contrary to ~~the~~ observations (Fig. 3b). Around 0300 UTC, a more sudden increase of TKE occur~~red likes~~, as in the observations but 30 min before and with a lower magnitude~~, even if it was underestimated~~. Then the simulated TKE remain~~ed quasi~~s almost constant around $0.7\ \mathrm{m^2\,s^{-2}}$ from 0400 UTC onwards~~around $0.7\ \mathrm{m^2\,s^{-2}}$~~, with a slightly higher variability than before. The model develop~~ed~~s similar TKE values at 10 m and 30 m, while ~~30 m~~ observed values ~~we~~are higher at 30 m.

Considering the radiative fluxes (Fig. 4), the increase of the LWD flux associated ~~to~~with fog onset ~~wa~~is simulated with a delay of 30~~-40~~ minutes, meaning that there ~~wa~~is a delay ~~o~~in the simulated formation of fog at elevated levels. After that, the LWD flux of $325\ \mathrm{W\,m^{-2}}$ ~~wa~~is correctly reproduced, indicating that the temperature and the optical thickness of the fog ~~we~~are fairly well simulated. Observations develop~~ed~~ a difference of $8\ \mathrm{W\,m^{-2}}$ between LWU and LWD during the fog life cycle, but the model fail~~ed~~s to reproduce this difference, leading to a slight underestimation of LWU. If the measurements ~~did~~do not ~~encounter an~~contain any errors, this probably means that the radiative properties of the simulated surface ~~we~~are not perfectly represented. A test on the emissivity of the surface (1 instead of 0.96) had no impact on the radiative fluxes, suggesting that the soil temperature was probably underestimated. After sunrise (0659 UTC), the downward and upward SW fluxes ~~were~~is gradually overestimated ~~by~~up to $15\ \mathrm{W\,m^{-2}}$, and LWD ~~were~~is slightly underestimated in a similar way due to the advanced dissipation time.

3.1.2 Microphysics

Considering the microphysical fields at 3 m agl, the onset of ~~LWC~~r_c higher than 0.001 ~~$\mathrm{g\,m^{-3}}$~~$\mathrm{g\,kg^{-1}}$ ~~was in agreement with the observations~~presents 30 min of advance (Fig. 5~~b~~a). Cloud droplets appear more than one hour before the observation but correspond to very low concentration (less than 10 per $\mathrm{cm^3}$) and negligible cloud mixing ratio. The delay identified on LWD flux increase ~~wa~~and on the temperature convergence is not reproduced on ~~LWC~~r_c, meaning that the time of formation of fog at the ground ~~wa~~is quite correctly reproduced (even with a small advance of 30 min) but the previous formation at elevated levels ~~wa~~is underestimated. This is corroborated by the LWP evolution (Fig. 5c), also characterized by a ~~4~~30 min delay compared to the Sirta ~~ponctual~~point observation, in agreement with LWD fluxes.

The increase of ~~LWC~~r_c during the development phase ~~was in agreement with the observed one but this phase was too long~~is too strong leading to an overestimation, with a maximum value of ~~$0.07\ \mathrm{g\,m^{-3}}$ instead of $0.035\ \mathrm{g\,m^{-3}}$~~$0.2\ \mathrm{g\,kg^{-1}}$ instead of the $0.03\ \mathrm{g\,kg^{-1}}$ observed. Then, during the mature phase, the slow decrease of ~~LWC~~r_c ~~wa~~is reproduced, ~~up to~~until ~~0830~~0900~~where both observed and simulated values became less than $0.001\ \mathrm{g\,m^{-3}}$~~. But as we have seen before, in reality, this first event of fog dissipation only concern~~ed~~s the levels very ~~near~~close to the surface~~ levels, as~~ and observed visibility at 18 m remain~~ed~~s less than 1300 m. ~~On the contrary~~In contrast, the fog ~~did~~does not reform~~ed~~ near the surface in the simulation, which induc~~ing~~es an advance of almost one hour on the dissipation time. The discrepancies between simulation and observation ~~was higher~~are greater on cloud droplet concentration than on ~~LWC~~cloud mixing ratio ~~during all~~throughout the fog life cycle, as the model strongly overestimate~~d~~s N_c, ~~up to~~by a factor ~~of~~that may be as high as ~~7~~14 (maximum values of ~~350~~700 $\mathrm{cm^{-3}}$ simulated against 53 $\mathrm{cm^{-3}}$ observed, Fig. 5~~a~~b). Maxima of N_c and ~~LWC~~r_c ~~occurred~~are reached at the same time, around 0300 UTC, th~~a~~en ~~both~~r_c decrease~~d~~s while N_c remains constant~~. But N_c increased again during the dissipation phase~~, before dropping sharply at the end of the fog.

The droplet size distribution (DSD) in the model is described by the normalized form of the generalized gamma distribution which gives a monomodal form (Fig. 5d). During the ~~formation phase (red lines)~~whole fog life cycle, the model overestimate~~d~~ ~~small~~s droplets with a diameter ~~between 2.5 μm and 7.5 μm~~larger than 4 μm and underestimates the smaller ones.~~and did not produce droplets of diameter larger than 9 μm. This trend continued during the fog life cycle (blue and then green line) even if it was less marked than at the initial stage. The model produced the largest droplets at the mature stage like in the observations, before reducing the spectrum during the dissipation. The simulated modes corresponded to 4 μm, 7.5 μm and 6 μm of diameters at the 3 stages. The overestimation of small droplets and the underestimation of larger ones leaded to the weakness of droplet sedimentation. Indeed, the surface cloud water amount by sedimentation is negligible after 12 hours of simulation (around 10^{-4}mm), while it reached 0.0674 mm by deposition.~~ The cloud water deposition rate at the ground presents a maximum of $0.36\ \mathrm{mm.day^{-1}}$ while the maximum of droplet sedimentation rate is $0.08\ \mathrm{mm.day^{-1}}$, meaning that the deposition is the main contributor to the cloud water amount at the ground.

~~The weakness of droplet sedimentation could partly explain the overestimation of N_c during all the whole fog life cycle, as well as the LWC, as it keeped too much water in the fog layer.~~

~~But another~~A reason that could explain the overestimation of droplet concentration and that will be developed in ~~the~~ Part 2 of this study, is that ~~the~~ equation (3)~~ allowing~~, which allows ~~to compute~~ the supersaturation peak value to be computed, does not take ~~into account~~ the sink term due to pre-existing ~~LWC~~r_c into account, as explained ~~in~~by Thouron et al. (2012). Due to the overestimation of simulated droplet ~~concentrations~~mass and number, ~~the Zhang~~all the diagnostics of visibility applied to simulated microphysical fields underestimate~~d~~ the observed visibility at 3 m and 18 m, especially the Zhang's formulation (Fig. 6). ~~The Gultepe formulation is better adapted to our simulation, reproducing correctly the visibility drop at the onset of the fog, while the visibility remained slightly underestimated during the fog life cycle.~~ As ~~LWC values are better reproduced~~r_c is less underestimated than N_c, the Kunkel formulation provides the least bad match~~ed~~ for ~~the~~ observations ~~the best~~. This explains why a simpler formulation of visibility based solely on r_c is usually more adequate given the difficulty of simulating N_c for the models.

The comparison between the REF simulation and observation for the set of parameters shows ~~a~~ fairly good agreement, even if there ~~we~~are some discrepancies. The main discrepancies ~~were, considering~~concerning the fog life cycle~~,~~ are an underestimation of the effect of elevated fog formation~~ and~~, inducing an advance of ~~1.5 h on~~30 min in the onset time near the ground and an advance of 1 h in the dissipation time. These elements are probably partly due to the semi-idealized representation of the Sirta surface in the simulation, and also to the comparisons with ~~ponctual~~point observations, ~~knowing~~given the horizontal variability ~~as~~that we will see ~~further~~below. Considering the microphysical fields, the main discrepancy ~~wa~~is an overestimation of the concentration of small droplets ~~concentration~~ near the ground~~,~~ and, to a less degree, of ~~LWC~~the cloud mixing ratio. They are felt to be acceptable and we can therefore consider that the REF simulation can be used to explore the processes driving the fog life cycle and to conduct sensitivity tests to try to reduce these discrepancies.

3.2 Vertical evolution

First the ~~fog~~ vertical evolution of the fog is analy~~z~~sed. Figure 7 represents the time ~~evolutions~~variations of vertical profiles of r_c and N_c, the radiative cooling rate and the vertical velocity in the updrafts, while parts a, c and d of Figure 8~~aed~~ represent~~s~~ the same time ~~evolution~~variation for total turbulent kinetic energy (resolved plus subgrid, noted TKE), and dynamical and thermal production of TKE for the REF simulation, all averaged over the horizontal area downstream the tree~~s~~ barrier. ~~As a preliminary comment,~~A first noteworthy feature is that subgrid kinetic energy is one order ~~less~~lower than resolved kinetic energy (not shown), meaning that the 5 m horizontal resolution allows an LES approach as most of the eddies are resolved.

The evolution of r_c ~~allows to decompose formally~~serves as a basis for decomposing the fog life cycle into the three phases: the formation, between 0200 and 03~~2~~00 UTC, until the fog bec~~ame~~omes optically thick; the development, between 0320 and 0~~7~~820 UTC, until r_c at upper levels of the fog layer beg~~an~~ins to decrease, and the dissipation from 0~~7~~820 UTC (Fig. 7a).

Before the fog onset and during the formation phase, the TKE ~~wa~~is small and spread over a 30 m layer that deepen~~ed~~s slowly~~, consecutively to the flow induced by~~ due to the tree~~s~~ barrier (Fig. 8a). TKE ~~was~~ mainly ~~produced~~occurs by dynamical production, which present~~ed~~s maxima at two levels~~,~~: near the surface and at 15 m height due to the trees (Fig. 8c). Thermal production ~~wa~~is negative due to the thermal stratification (Fig. 8d). The radiative cooling near the ground (Fig. 7c) and the mixing by the tree drag effect ~~we~~are the ingredients ~~allowing the apparition of~~that allow fog to appear at ~~elevated level~~the same time over a 30 m deep layer (Fig. 7a). Then the mixing by the tree~~s~~ barrier cause~~d~~s ~~a subsiding effect of~~ the fog layer ~~down to the ground and a vertical development above~~to develop vertically at greater heights (Fig. 7a). Hence, the effect of elevated formation ~~wa~~is reproduced, even if the height of fog onset ~~wa~~is underestimated (150 m given by the ceilometer and 30 m in the simulation)~~. T~~, and the period ~~of subsiding effect of~~during which the fog subsides to reach the ground ~~wa~~is ~~therefore shorter and equal to 20 min~~almost instantly. During this first phase, mean updraft vertical velocities ~~we~~are small, up to $0.15\,\mathrm{m\,s^{-1}}$ ~~(not shown)~~(Fig. 7d), in agreement with Ye et al. (2015), who observed a vertical velocity of $0.1-0.2\,\mathrm{m\,s^{-1}}$ in a fog layer between 40 m and 220 m ~~depth~~deep in China. Considering Eq.3 for supersaturation evolution with the two source terms ~~function of~~depending on vertical velocity and radiative cooling, the activation of fog droplets ~~was~~ during the fog formation ~~fog~~is mainly produced by radiative cooling at the top of the fog layer (Fig. 7b and c).

At the beginning of the development phase (around 03~~2~~00 UTC), when the fog depth reache~~d~~s approximately 80 m, it bec~~ame~~omes optically thick to longwave radiation. ~~E~~At exactly ~~at~~ that time, TKE increase~~d~~s significantly by dynamical production (Fig. 8a and c), in agreement with Nakanishi (2000)~~, meaning~~'s findings, which indicates a dynamical change. The optical thickness of the fog layer cause~~d as~~ strong radiative cooling at the top of the ~~fog~~ layer, ~~higher~~greater than $5.5\,\mathrm{K\,h^{-1}}$ (in absolute value, Fig. 7~~d~~c), and ~~LWC~~r_c values bec~~a~~ome stronger in the upper part of the fog layer. Hence, the fog top bec~~a~~omes the location of the dominant processes with radiative cooling. It induce~~d~~s small downdrafts and buoyancy reversal. ~~Additionally~~In addition to the vertical velocity of the updrafts now higher than $0.2\,\mathrm{m\,s^{-1}}$ ~~in all~~throughout the fog layer, a second maximum of droplet concentration of ~~1000~~1100 $\mathrm{cm^{-3}}$ occur~~red~~s in the upper part of the fog layer around 0320 UTC. The sudden optical thickening correspond~~ed~~s to the increase of surface LWD ~~up~~ to $320\,\mathrm{W\,m^{-2}}$ (Fig. 4) and to ~~the~~ maximum ~~of~~ cooling at the ground (Fig. 2a). ~~In~~At the same time, temperatures converge~~d~~ ~~between~~in the vertical levels near the ground ~~(Fig. 2a and b)~~, showing the effect of fog on the stability profile as analy~~z~~sed by Price (2011).

Then, during the development phase, the top of the fog layer ~~wa~~is characterized by vertical wind shear inducing ~~a~~ positive dynamical production of TKE, while small values of positive thermal production appear~~ed~~ at the top due to buoyancy reversal. Inside the fog layer, in the ~~40~~ lowest 40 m~~etres~~, the drag effect of the trees induce~~d highers~~s values of kinetic energy higher than $0.6\,\mathrm{m^2\,s^2}$. The maximum of r_c continue~~d~~s to increase in the upper part of the fog layer up to 0500 UTC, reaching 0.3~~5~~7 $\mathrm{g\,kg^{-1}}$ at 120 m (Fig. 7a). ~~In~~At the same time, LWD surface fluxes remain~~ed~~ constant while the fog layer continue~~d~~s to deepen and the LWP continues to increase ~~up to~~until 0500 UTC (Fig. 5c).

Around ~~0430~~-0500 UTC, a change occur~~red~~s ~~o~~in the development of the fog layer: it continue~~d~~s to thicken, but at a ~~smaller~~slower rate, while the LWP beg~~an~~ins to decrease in the simulation. This change of growth at the top of the fog layer ~~wa~~is associated ~~to~~with a warming in the fog layer (not shown) and a decrease of the maximum radiative cooling near the top ~~that~~which spreads over a ~~broader~~greater depth (Fig. 7c). This also correspond~~ed~~s ~~also~~ to an increased number of resolved updraughts and downdraughts near the top (Fig. 7d). ~~V~~The variability of the fog depth also bec~~ame~~omes ~~also~~ stronger, ~~linked to~~in connection with fog-top waves as we will see ~~further~~below. This change of growth seems to be linked to the fact that the fog layer reache~~d~~s the top of the nocturnal boundary layer, meeting stronger temperature, humidity and wind gradients. This increase~~d~~s the top entrainment process, limiting the deepening of the fog layer. With the decrease of the top radiative cooling, cloud droplet concentration bec~~ame~~omes ~~quasi~~more homogeneous in the fog layer, except near the ground where it decrease~~d~~s by deposition. In the same way, the cloud mixing ratio also beg~~an~~ins to decrease ~~also~~ near the ground (Fig. 7b).

The beginning of the dissipation phase in the simulation(around 0~~7~~820 UTC) ~~can be identified~~is preceded by the beginning of solar radiation, and divergence between surface LWU, which start~~ings~~ to increas~~ing~~e, and surface LWD, starting decreasing ~~in the simulation~~ (Fig. 4). The dissipation of the fog beg~~an~~ins at the surface, and the fog lift~~ed~~s into a stratus layer. The radiative heating of the surface ~~increased~~induces the convective structure of the fog as vertical velocity in the updrafts increase~~d~~s (Fig. 7~~b~~c and d) and thermal production of TKE bec~~ame~~omes significantly positive (Fig. 8d). Additionally, after sunset, downdraughts at the top of the fog layer increase~~d~~ the amount of solar radiation reaching the ground and feeding the heating at the base of the fog layer. Hence, near the ground, both thermal and dynamical effects contribute~~d~~ to the production of TKE, and to a deepening of the TKE layer ~~up~~ to 60 m. The height of the fog top continue~~d~~s to increase as it ~~wa~~is driven by radiative and evaporative cooling inducing vertical motions and top entrainment. ~~If~~Although mixing ratio decrease~~d~~s at all levels, droplet concentration increase~~d~~s sharply when the fog layer lift~~ed~~s from the surface (Fig. 7b). As the cloud evolve~~d~~s into a stratus layer, droplet activation ~~wa~~is no ~~more~~longer induced by radiative cooling at the top of the fog layer but by updraft vertical velocity ~~in all the~~at all cloud depths, and especially near the stratus base. The stronger vertical velocity ~~(Fig. 7d) allowed to~~ activates more droplets for the same water content ~~amount~~. Droplets bec~~a~~ome smaller and more numerous, preventing the droplet sedimentation process and limiting the decrease of LWP~~, while~~. Moreover, the deposition process ~~wa~~is no~~t~~ longer active ~~any more~~ ~~without~~as there are no cloud droplets at the surface. We will now consider the horizontal heterogeneity of the fog layer.

3.3 Horizontal variability

To better characterize turbulent structures and the impact of trees on the fog layer, the horizontal variability of the fog layer is examined. Figure 9 presents horizontal and vertical cross-sections of wind speed, cloud mixing ratio, potential temperature and TKE at 02~~4~~10 UTC during the formation phase. The tree~~s~~ barrier induce~~d~~s a blocking effect of the flow upstream, and enhance~~d~~s the turbulence by wind shear downstream, accelerating the flow near the ground and creating longitudinal structures in the direction of the wind. Ascents occur~~red~~ upstream and small subsidence downstream, up to 2 $\mathrm{cm\,s^{-1}}$ (not shown), ~~drawning~~brings warmer and dryer air from above to the ground. Therefore structures of stronger wind near the ground downstream coincide~~d~~ with structures of warmer ~~and~~, clear air as they delay~~ed the~~ fog formation. The fog form~~ed~~s at the surface upstream ~~from~~of the trees, and 500 m far downstream, while it appear~~ed~~s first at elevated levels ~~between both~~over the intermediate area between the trees and far downstream (Fig. 9d). The fog t~~ook~~akes about 1 hour to cover the entire domain at ground level. Thus, heterogeneity of the surface vegetation explains heterogeneities ~~o~~in fog onset over the Sirta site, as well as the fog property ~~to~~of developing ~~fog~~ first at elevated levels. After the formation phase, the base of the fog layer ~~standed~~is at the ground over the whole domain. These results are in agreement with the effects of building ~~effects~~ on fog studied by Bergot (2015b) who found a 1.5 hour period of heterogeneity of fog formation over the airport area.

During the development phase, as shown on the vertical cross-sections of Fig. 10 at 0620 UTC, horizontal rolls appear~~ed~~ at the top of the fog layer and ~~we~~are associated ~~to~~with dynamical production of TKE by shear. They ~~we~~are aligned almost perpendicularly to the mean wind direction (not shown). These structures correspond to Kelvin-Helmotz (KH) instability, already observed by Uematsu et al. (2005) and modelled by Nakanishi (2000) and Bergot (2013). They ha~~d~~ve depth corresponding to about one third of the fog layer height, ~~like~~as in Bergot (2013), and a horizontal wavelength of the order of 500 m. These horizontal rolls explain the oscillations at the top of the fog layer visible ~~o~~in Fig. 7 and Fig. 8. They bec~~a~~ome well marked from ~~0430~~0500 UTC when the depth of the fog layer beg~~an~~ins to increase more slowly, as the fog layer reache~~d~~s the top of the nocturnal boundary layer, meeting stronger wind gradients~~ (not shown)~~. They induce~~d~~ strong horizontal variability of cloud mixing ratio near the top of the fog, with larger values in the ridges of the fog-top rolls, and smaller ones in the troughs (Fig. 10a). Local updraughts occur~~red~~ upstream of the crest of the wave, and downdraughts downstream, both up to $1.2\ \mathrm{m\,s^{-1}}$ (Fig. 10d). Maximum of droplet concentration occur~~red~~s near the top of the fog layer (Fig. 10b) in the radiative cooling layer (Fig. 10c), and preferentially upstream the crest of the wave rather than downstream, in the ascent area, where the~~y we~~droplets are preferentially activated and transported. These extrema of droplet concentration do not appear ~~o~~in Fig. 7 as they ~~we~~are hidden by the spatio-temporal average.

Inside the fog layer, the radiative cooling ~~wa~~is negligible while vertical velocity present~~ed~~s strong spatial heterogeneities. Maxima of supersaturation appear~~ed~~ to be strongly correlated with vertical velocity (Fig. 10e), with values up to $0.2\underline{7}5\%$ which ~~we~~are probably overestimated~~ even if~~, although this cannot be confirmed as measurements of supersaturation peaks ~~we~~are not available beyond the surface. ~~But~~However droplet concentration ~~was quasi homogeneous over the horizontal domain~~variations are smooth, and d~~id~~oes not show a strong correlation ~~to~~with the maximum supersaturation, due to the pre-existing droplets.

Near the ground, maximum simulated values of supersaturation l~~ay~~ie around 0.1% while Hammer et al. (2014) and Mazoyer et al. (2016) reported observed supersaturation peaks lower than 0.1%. The presence of trees and the deposition process induce~~d~~ smaller droplet mixing ratio and concentration near the surface.

During the dissipation phase, heterogeneities remain at the top of the fog layer, but the signature of KH waves disappear~~ed~~s (not shown). The dissipation of fog at ground level t~~ook~~akes about 20 minutes, and, as noted in Bergot et al. (2015a), d~~id~~oes not reveal a clear effect of surface heterogeneity~~, as well as in Bergot et al. (2015a)~~.

Having characterized vertical and horizontal heterogeneities of the fog during its life cycle, sensitivity tests are now presented to identify the sources of variability and their impact on the microphysical fields.

4 Sensitivity study

In order to better characterize the physical processes dominating the fog life cycle and driving the microphysical properties, sensitivity tests ~~a~~were conducted in a second step. The resulting simulations are summarized in Tab.1, considering their difference with the REF simulation.

4.1 Impact of trees

To evaluate the impact of trees on the dynamics and on the microphysics of the fog, a simulation called NTR ~~has been~~was run, ~~where the~~in which the barrier of tree was replaced by grass~~ has replaced the barrier of trees~~. ~~Hence~~So, deposition on the grass

~~i~~was considered over the whole domain. Fig. 3a shows that, w~~W~~ithout trees, the 10 m wind speed ~~wa~~is overestimated over the instrument~~al~~ed area~~ (Fig. 3a)~~. As in REF but 30 min earlier, the model develop~~ed~~s a sudden increase of TKE ~~at 0300~~around 0230 UTC at the beginning of the development phase, meaning that this change ~~wa~~is linked to the increase of the optical thickness~~,~~ and not to the turbulence induced by trees (Fig. 3b and Fig. 8b). ~~But a~~After this period, TKE ~~wa~~is underestimated and remain~~ed~~s stronger at 10 m height than at 30 m, contrary to observation, which means that the drag effect of trees ~~wa~~is responsible ~~of~~for the observed stronger TKE at 30 m height. The fact that the REF simulation develop~~ed~~s ~~quasi~~very similar TKE at 10 m and 30 m agl probably means that the representation of surface heterogeneities ~~wa~~is still underestimated, which can be explained by the broad range of surface covers present in reality, in addition to the trees (lake, small buildings~~...~~, etc.)~~,~~ but not included in the simulation.

The main differences ~~o~~in dynamics between NTR and REF appear~~ed~~ first on total TKE, with ~~the absence of stronger values in the first 40 metres in NTR, as they were restricted to the immediate vicinity of the ground~~a thinner layer of TKE values higher than $0.5\ \mathrm{m^2\,s^{-2}}$ and smaller maxima (Fig. 8b). Before the fog formation, the too~~-~~thin layer of turbulence near the ground in NTR limit~~ed~~s the supply of warmer air from above, inducing an overestimation of the vertical temperature gradient before the fog, and emphasizing the cooling in the low levels, with 2 K less than in REF (Fig. 2c). Figure 11a presents the temporal evolution of cloud mixing ratio vertical profiles during the NTR simulation, to be compared to Fig. 7a ~~and b ~~for REF, and Figure 12a and b exhibit~~ed~~ instantaneous vertical cross sections of potential temperature at the fog formation with REF and NTR. The stronger cooling with NTR homogen~~e~~ize~~d~~s the fog formation at the ground and prevent~~ed~~s elevated fog formation. The consequence is that the onset of fog with NTR occur~~red~~s almost 2 hours ~~before the~~earlier than actually observ~~ation~~ed and than in the REF simulation (Fig. 2d). Fig. 13 summarizes the impact of sensitivity tests on the microphysical fields and NTR (purple lines) can be compared to REF (red lines) in Fig. 13~~abc~~a b and c. During the formation and ~~the ~~development phases, the ~~depth of the ~~fog layer ~~wa~~is thinner in NTR than in REF~~,~~ because of the formation at the ground and the absence of mixing without trees, thus limiting the vertical development. ~~M~~The maximum of cloud mixing ratio with NTR ~~wa~~is increased compared to REF, due to the absence of warming by entrainment, ~~leading~~and leads to ~~a cooling ~~largely overestimated cooling near the ground ~~when compared~~in comparaison to observations (Fig. 13a). Therefore the Kunkel diagnostic underestimate~~d~~s the visibility much more than REF, as ~~well as~~do the other diagnostics (Fig. 6d). Inside the fog layer, despite the increase of r_c, the positive temporal evolution of N_c, called the production of N_c,~~wa~~ is not higher than in REF (Fig. 11b), as smaller vertical velocities and higher cloud mixing ratio production compensate~~d~~ for the stronger cooling in the activation process.

Additio~~n~~nally, near the ground, droplet concentration ~~wa~~is even smaller than in REF, as deposition~~ effect~~, acting only at the first vertical level in NTR, ~~wa~~is active ~~since~~from the onset of the fog, due to the absence of elevated formation and to the thinner fog layer. Consequently, the DSD at 3 m shift~~ed~~s towards larger droplets in NTR (Fig. 13c), consistently with the reduction of droplet concentration.

Also, during the development phase, 500 m wavelengths of KH waves ~~we~~are more smooth and regular without trees~~ (Fig. ??)~~ and this ~~has been~~is noted during~~ all~~ the whole phase. This ~~can be~~is shown on kinetic energy spectra applied ~~on~~to vertical velocity over the whole fog depth, computed according to Ricard et al. (2013) and presented ~~o~~in Fig. 14. The spectra of REF and NTR present~~ed~~ two main differences: firstly the TKE variance ~~wa~~is smaller with NTR at wavelengths ~~finer~~shorter than

200 m, meaning that the flow present~~ed~~s ~~less~~fewer fine scale structures without the tree drag effect~~. S~~ and, secondly, the peak of variance at 500 m wavelength, corresponding to the KH waves, ~~wa~~is more pronounced ~~with~~in NTR.

~~The regular KH waves with NTR induced a regular wave pattern of the radiative cooling layer at the top of the fog layer (Fig. ??c). Therefore, higher droplet concentrations were spread over a deeper layer at the top of the fog with NTR than with REF (Fig. ??b). This is also emphasized by the fact that the pre-existing cloud water content, higher with NTR than with REF, is not taken into account in the diagnostic of maximum supersaturation as it should be. Comparing Fig. ?? to Fig. 10, it also appears that vertical velocity associated to KH waves at the top of the fog were smaller with NTR than with REF, but this was not systematic during the period. However, the intensity of vertical velocity at the top of the fog layer seems to be correlated towith the depth of the KH waves. Hence, it appears that surface heterogeneities relative to the trees introduced small perturbations up to the top of the fog layer on this case, that modifiedy the regular wave pattern but that did not remove the KH waves.~~

~~During the dissipation phase, KH waves at the top of the fog layer remained longer in NTR as the dissipation time was delayed (not shown). This time lag was in better agreement with the observations, unlike the rest of the fog life cycle.~~

To summarize, the absence of tree~~s~~ barrier produce~~d~~s an unrealistic simulation, as it ~~induced a~~causes the fog onset to occur too early ~~onset of fog~~ (almost 2 hours ~~of~~in advance)~~, a too strong~~. It also induces cooling that is too strong in the low levels, and a large overestimation of the near surface ~~LWC~~cloud mixing ratio ~~during all~~throughout the fog life cycle, damaging the visibility. On the other ~~side~~hand, droplet activation ~~wa~~is reduced near the ground due to smaller vertical velocities and to a stronger impact of surface deposition, shifting the DSD to larger droplets. ~~It~~The absence of trees also modifie~~d~~s the signature of the KH waves at the top of the fog layer, with a more regular pattern and ~~less~~fewer small scale heterogeneities~~ on the microphysical fields near the top of the fog layer~~. The impact of the deposition process will now be examined more precisely.

4.2 Impact of deposition

~~Two~~Three simulations ~~have been~~were carried out to better characterize the role of the deposition process, both keeping the tree~~s~~ barrier. The first one, called NDT, removed only deposition over trees compared to REF, considering that trees acted as grass for deposition. This was done by activating deposition only at the first level of the model. The second one, called NDG, remove~~d~~s ~~fully~~ deposition altogether. The third one, noted DE~~5~~8, considered a deposition velocity V_{DEP} of ~~5~~8 $\mathrm{cm\,s^{-1}}$ over grass and trees, which is the upper bound given by Katata (2014) instead of 2 $\mathrm{cm\,s^{-1}}$ ~~like~~as in REF. Figure 13~~abc~~a, b and c compare~~s near surface~~ 3 m microphysical fields, and Figure 15a the LWP.

NDT very slightly increase~~ds slightly~~ droplet mass and number downstream of the tree~~s~~ barrier, ~~as well as~~and the LWP during the fog life cycle (Fig. 15). ~~But~~Conversely, removing deposition everywhere with NDG ha~~d~~s a considerable impact as it increase~~ds by a ratio of 8~~ the cloud mixing ratio and the concentration near the surface by a factor between 2 and 3. With NDG, the onset of fog occur~~red~~s at the surface and not ~~at elevated levels~~on a 30 m deep layer, almost 2 hours ~~before~~earlier than in observations and in the REF simulation (Fig. 11c). During the development phase, there is no longer a vertical gradient of r_c and N_c ~~has disappeared~~ (Fig. 11c and d)~~, even if radiative cooling at the top was stronger with higher cloud mixing ratio (with maxima of cooling more than −8 K h−1)~~. The temporal evolution of cloud droplet concentration in the fog layer shows constant vertical profiles, without maxima during the formation and the dissipation phases ~~like~~, as in REF. Hence, cloud droplet concentration ~~wa~~is constant during the fog life cycle near the ground, while observations report~~ed~~ a decrease during the development phase (Fig. 13~~a~~b). NDG also develop~~ed~~s ~~also~~ a broader DSD, with more ~~numerous large~~ droplets with a diameter larger than 4 μm. ~~Therefore, droplet sedimentation was significantly increased as NDG reported a mean cumulated cloud water amount of 0.053 mm reaching the surface during the 12 hours by sedimentation, while the REF simulation produced 0.067 mm of cloud water at the surface after 12 hours, the sedimented water being negligible.~~ The fog layer ~~wa~~is ~~also~~ deeper ~~during all~~throughout the life cycle, and therefore the LWP ~~wa~~is largely overestimated with a maximum between 0500 and 0600 UTC, of about twice the observed value (Fig. 15). Due to the larger amount of cloud water near the ground, the dissipation at the ground ~~wa~~is delayed by more than one hour. Moreover, NDG reports a maximum cumulated cloud water amount reaching the ground of 0.053 mm after the 12 hours by sedimentation, while the REF simulation produces a maximum of 0.074 mm by deposition and sedimentation. Even if NDG produces higher LWP over a longer period and higher concentration of large droplets than REF, the cloud water amount reaching the ground is lower, meaning that a deposition velocity of 2 $\mathrm{cm\,s^{-1}}$ is more efficient than the sedimentation process to collect cloud water at the ground.

~~Another test, noted DE5, considered a deposition velocity V_{DEP} of 5 $\mathrm{cm\,s^{-1}}$ instead of 2 $\mathrm{cm\,s^{-1}}$ like in REF (Fig. 13abc and Fig. 15a). It~~In contrast, DE8 induce~~d~~s a ~~slight diminution~~significant reduction of the near surface ~~LWC~~r_c, N_c and the LWP, ~~but the fog life cycle, the droplet concentration and the LWP remained almost unchanged~~and the onset of fog near the ground coincides relatively well with the observation. The formation of fog at elevated levels is more pronounced, and r_c over the whole fog depth is reduced during the development phase compared to REF (Fig. 11d and e). With DE8, the cloud water deposition rate at the ground presents a maximum of $0.48\ \mathrm{mm.day^{-1}}$ during the period while the maximum of droplet sedimentation rate is $0.02\ \mathrm{mm.day^{-1}}$. Among the different simulations conducted in this study, the performance of DE8 to reproduce the microphysical fields is the best. This means~~meaning~~ that the deposition process is ~~not too~~ highly sensitive to the deposition velocity.

Zhang et al. (2014b) ha~~d~~ve already shown that ~~taking into account~~including a deposition term in simulations seem~~ed~~s to have some effect on the droplet concentration in the layer near the ground and consequently on visibility~~. B~~ but their effect was less pronounced than here. A possible explanation is that both $u*$, the friction velocity, and the mean volumetric diameter of droplets~~, taken into account~~ used in their parametrization, were underestimated. In our case, the deposition process, even with a simple parametrization, appear~~ed~~s to be essential to correctly simulate the fog life cycle and to ~~be closer to~~approach the observed microphysical values near the ground more closely. It impact~~ed~~s ~~significantly~~ the microphysical fields significantly. Hence, ~~the remove of~~neglecting this process ~~induced~~increases droplet sedimentation~~,~~ but in insufficient quantity to avoid unrealistic droplet concentration and cloud mixing ratio in the fog layer and near the surface. It also modifie~~d~~s the fog life cycle in terms of onset and dissipation times, LWP and microphysical characteristics inside the fog layer. The~~, and prevented~~ elevated fog formation, which ~~wa~~is a climatological characteristic of the Sirta site, is the result of the tree drag effect, which mixes the lowest levels, and the deposition process, which erodes the near-surface water content. We will now examine the impact of the horizontal resolution ~~to~~on the simulated fog life cycle.

4.3 Sensitivity to effective resolution

In order to assess the impact of spatial resolution on the fog life cycle, a 2 m horizontal resolution (called DX2) was carried out using the same momentum advection scheme ~~than~~as in REF (CEN4TH). According to Skamarock (2004), kinetic energy (KE) spectra deduced from simulations allow ~~to set up~~ the effective resolution to be set up as the scale ~~from~~at which the model starts to depart~~s~~ from the theoretical slope, which is -3 for vertical velocity spectra applied to stable turbulence. Mean KE spectra applied to the vertical wind component reveal~~ed~~ effective resolution of the order of $4-5\ \Delta x$ for simulations with CEN4TH (DX2 and REF), in agreement with Ricard et al. (2013), namely 8 m and 20 m respectively (Fig. 14).

With DX2, top entrainment ~~wa~~is more active as updrafts and downdrafts ~~we~~are represented at finer resolution, limiting the cooling near the surface (Fig. 12d) and the vertical development of the fog. The cloud mixing ratio near the ground is slightly reduced, but the droplet concentration is almost unchanged, inducing a shift of the mode of the DSD to 7 μm instead of 8 μm (Fig. 13d, e and f). ~~Only small droplets were more numerous, increasing slightly droplet concentration during all the fog life cycle (Fig. 13d and f).~~ The fog onset ~~and dissipation times and the LWC were almost unchanged~~time is set a bit later and the dissipation time a bit sooner (Fig. 13e), and the LWP ~~wa~~is slightly reduced compared to REF (Fig. 15b)~~ but~~. ~~The close results~~But the differences between DX2 and REF ~~are~~remain quite small in agreement with the convergence ~~in stable conditions~~ around 2 m resolution in stable conditions already shown by Beare and MacVean (2004).

~~Then~~In two other tests ~~have been held~~performed on the wind transport scheme, keeping the 5 m horizontal resolution~~:~~, the CEN4TH scheme ~~has been~~was replaced by the WENO (Weighted Non-Oscillatory, Shu (1998)) scheme at 3rd order (called WE3) or 5th order (called WE5). These spatial schemes, associated ~~to~~with an Explicit Runge-Kutta temporal scheme, allow time steps 10 times larger than CEN4TH associated ~~to~~with a Leap-Frog temporal scheme, but they were run here with the same small time step (0.1 s) for ~~the~~ comparison. Due to the upstream spatial discretization, WENO schemes ~~we~~are implicit~~e~~ly diffusive and ~~we~~are therefore characterized by a coarser effective resolution, especially WENO3 due to its lower order~~:~~. Fig. 14 shows that the effective resolutions ~~we~~are 35 m (i.e. 7 Δx) and 70 m (i.e. 14 Δx) for WE5 and WE3 respectively~~ (Fig. 14)~~. WE3 significantly reduce~~d~~s ~~significantly~~ the top entrainment and the supply of warmer~~ and~~, dryer air from above~~,~~. This empha-siz~~ing~~es the cooling near the surface (Fig. 12c)~~. Indeed,~~ as the diffusive contribution of the advection operator dissipate~~d~~s small updrafts and suppresse~~d as~~s part of the resolved kinetic energy variance, in particular ~~the one~~that present at the top of the fog layer. This induce~~d~~s an overestimation of the thermal gradient near the surface before the fog, and ~~a too strong~~leads to cooling that is too strong by 1 K during the fog (not shown). The consequences of the ~~enhanced~~increased cooling ~~we~~are that the onset of fog at the surface ~~happened~~occurs 1.5 h ~~before~~earlier than actually observ~~ationed (with an initial formation at elevated levels that is not shown)~~, the ~~LWC~~r_c ~~during all the fog life cycle wa~~is largely overestimated throughout the fog life cycle, and the dissipation ~~timewa~~is delayed (Fig. 13e). The DSD ~~moved towards~~is characterized by higher concentrations of larger droplets (Fig. 13.f). ~~It increased the droplet sedimentation as the mean cloud water content reaching the surface by sedimentation was 4.10^{-4} mm after 12 hours of simulations, that is 4 times more than in REF, compared to 0.1 mm by deposition for WE3.~~ Considering the microphysical fields, WE3 tends to be closer to NTR simulation, meaning that a diffusive transport scheme ~~dilutes significantly~~significantly diminishes the tree drag effect.

~~On the contrary~~In contrast, the differences ~~were very small~~ between WE5 and REF are very small: only the LWP ~~wa~~is ~~a bit~~ higher with WE5 during the dissipation phase due to a ~~fog slightly deeper~~slightly deeper fog layer. This underlines the less diffusive behaviour of WENO5 and its higher accuracy compared to WENO3.

Thus the jump ~~o~~in the effective resolution with the diffusive WENO3 scheme affect~~eds significantly~~ the fog life cycle significantly, while the smaller deviation with WENO5 ha~~d~~s almost no impact. Increasing numerical implicit diffusion seem~~ed~~s to have almost ~~similar than~~the same effect as removing the drag effect of trees. This ~~has~~ also underline~~d~~s the importance of the numerical schemes ~~in order to~~for correct~~ly~~ handl~~e~~ing of the cloud edge problem (Baba and Takahashi, 2013). ~~As well a 2 m horizontal resolution instead of 5 m did not bring important changes. Finally, sensitivity tests on initial fields are presented.~~

4.4 ~~Sensitivity to initial conditions~~

~~This test was designed to see whether the initial humidity field could reduce the bias on microphysical fields. Two simulations were considered. In the first, called HM2, the relative humidity of the initial profile in the boundary layer was reduced by 2%, and, in the second, called HP3, the relative humidity of the initial profile was increased by 3% over the same depth. In Fig. 13g, h and i, it appears that the fog life cycle is significantly modified, with a fog onset time deviating from the observations : it occurs around 2 hours earlier with HP3 and 2 hours later with HM2. However 3 m r_c is almost the same during the development and mature phases. Also neither of the simulations changes the DSD or the droplet concentration extrema. The LWPs of REF, HM2 and HP3 are superimposed (Fig. 15c) during the mature phase, so the dissipation time is unchanged.~~

~~It appears that taking away some humidity in the initial state does not reduce the droplet concentration, and the overestimation of the droplet concentration cannot be explained by an inadequate initial humidity profile.~~

~~Sensitivity tests were also conducted for surface temperature (+ − 2 K) and humidity (+ − 10%), but had very small effects on the fog life cycle and on the microphysical fields (not shown).~~

~~The last test involved an increase (VP3) or a decrease (VM3) of the wind speed in the free atmosphere in the initial and forcing conditions. In Fig. 13g, h and i, it can be seen that the lower the wind, the earlier the formation time, the higher the r_c and the later the dissipation time, as the mixing with higher dry, warm air is reduced. In contrast, a stronger wind drastically reduces the duration of the fog life cycle and the surface r_c. VM3 succeeds in broadening the droplet spectrum, but the extrema of the droplet concentration do not change significantly.~~

~~Thus, all the tests presented in Figures 13 and 15 fail to reduce the droplet concentration compared to REF. Only the NTR simulation reduces it somewhat, due to a broader droplet spectrum, but it overestimates the r_c and advances the fog onset. This probably means that modifying the dynamical conditions is not a way to improve the droplet concentration prediction further, considering the improvement brought by the deposition process.~~

5 Conclusion

Large eddy simulations of a radiation fog event observed during the ParisFog campaign were performed, with the aim of studying the impact of dynamics on microphysics. In order to study the local structures of the fog depth, simulations were performed at 5 m resolution on the horizontal scale and 1 m on the vertical scale near the ground, and included a tree~~s~~ barrier present near the instrument~~al~~ed site, taken into account in the model ~~with~~by means of a drag approach. The model included a 2-moment microphysical scheme, and a deposition term was added to the droplet sedimentation, representing the ~~droplets~~ interception of droplets by the plant canopies and acting only at the first vertical level above grass, and ~~over~~above the height of the trees.

The performance of the reference simulation was satisfactory as there was ~~a~~ fairly good agreement with the classical near-surface measurements. The main discrepanc~~y~~ies w~~as~~ere an overestimation of the concentration of small droplets ~~concentration~~ near the ground, ~~to a less degree~~ of liquid water content, and an advance on the dissipation time of ~~little more than~~ one hour. Th~~e~~is good performance allowed ~~to explore~~ the processes driving the fog life cycle to be explored.

The formation of the fog at elevated levels and the ~~rapid subsiding effect of the fog layer down to the ground just after, that is~~fact that it subsided to the ground in a very short time, a frequently observed characteristic of radiation fog events at the Sirta site, has been elucidated as a consequence of the tree drag effect ~~as~~when the wind ~~overcame~~met this obstacle and the deposition effect which reduces the formation of droplets near the surface. In contrast, the fog formed at the surface first upstream ~~from the trees~~ and 500 m downstream of the trees, leading to a duration of about one hour ~~of duration~~ for ~~the~~fog formation at the surface over the whole domain.

At the beginning of the development phase, the fog became optically thick to longwave radiation, inducing a significant increase of kinetic energy by dynamical production, ~~and that~~which was also associated ~~to~~with temperature convergence at low levels. The radiative cooling near the top of the fog layer was the main source of droplet activation so ~~that~~ the droplet concentration was maximum in the upper levels of the cloud.

During the development phase, ~~a slower growth of~~ the fog layer depth ~~occurred~~grew more slowly when the fog ~~layer~~ reached the top of the nocturnal boundary layer, ~~meeting~~encountering stronger thermodynamical ~~and dynamical~~ gradients and wind shear. Horizontal rolls at the top of the fog layer, associated ~~to~~with Kelvin-Helmotz instabilities, became ~~well-marked~~prominent. The cloud droplet concentration became quasi homogeneous in the fog layer ~~on time~~when averaged over time b~~. B~~ut ~~locally,~~ extrem~~a~~es of droplet concentration occurred locally near the top of the fog in the radiative cooling layer, with maxima preferentially upstream of the crests of the waves rather than downstream, in the ascent area~~, meaning that mainly~~. This indicates that vertical velocity ~~and secondly~~makes the main contribution to droplet activation at the top of the fog layer, followed by the contribution of radiative cooling ~~contribute to droplet activation at the top of the fog layer~~. Inside the cloud layer, maxima of supersaturation were directly linked to the local updrafts, while variations of~~the~~ droplet concentration ~~remained almost homogeneous~~were smoother.

During the dissipation phase, as the fog ~~in~~evolved into a stratus layer, the cloud mixing ratio decreased at all levels ~~but~~. However, a sharp increase ~~of~~in the droplet concentration occurred over the whole depth of the cloud ~~as~~because droplets were now only activated by the convective ascents ~~at the base of the stratus~~.

~~Then different~~Various sensitivity tests ~~provide a better understanding of the physical processes involved during the fog life cycle~~allowed to identify the main processes affecting the evolution of fog. The tree drag effect and the deposition process were considered as essential to correctly reproduce the main characteristics of the fog. The absence of the tree~~s~~ barrier produced an unrealistic fog simulation, with ~~a~~ too early an onset, ~~a too~~excessively strong cooling and a large overestimation of the near-surface ~~LWC~~r_c, ~~damaging the visibility diagnostic~~worsening visibility diagnosis. ~~It also modified the signature of the KH waves at the top of the fog layer, with a more regular pattern shown on energy spectra.~~

~~The removal of~~Neglecting the deposition process over ~~all the~~the whole vegetation canopy exerted the most significant impact on the fog prediction, as it produced more unrealistic water content near the surface, prevented elevated fog formation, ~~but~~and also modified the fog life cycle and suppressed vertical and temporal heterogeneities of the microphysical fields. Conversely, increasing the droplet deposition velocity from $2\ \mathrm{cm\,s^{-1}}$ to $8\ \mathrm{cm\,s^{-1}}$ reduced significantly the cloud mixing ratio near the surface and the droplet concentration.

Increasing the horizontal resolution ~~up~~ to 2 m did not change ~~significantly~~ the fog prediction significantly, ~~meaning~~which means that ~~a~~ grid convergence seems to be achieved at these resolutions. Conversely, increasing the numerical diffusion with a momentum transport scheme of lower order, ~~which involves~~involving a coarser effective resolution, ~~limited~~ drastically limited the top entrainment, and tended ~~almost to~~strongly towards the solution where the tree drag effect was ignored, underl~~y~~ining the importance of the properties of numerical schemes in LES, ~~in~~ particularly at cloud edges.

~~Lastly~~Other tests, not presented here, modifying the initial conditions in terms of humidity or wind profiles, impacted the fog life cycle but failed to reduce ~~much more the~~the overestimated droplet number concentration. This means that taking away some humidity in the initial state did not reduce the droplet concentration, and the overestimation of the droplet concentration could not be explained by an inadequate initial humidity profile.

This study demonstrates the feasibility and the interest of LES including surface heterogeneities to improve our understanding of ~~the~~ fog processes. At these fine resolutions, surface heterogeneities have a strong impact~~ which~~, explain~~s a~~ing part of the variability in the fog layer~~. T~~ and making these simulations ~~remain~~ very challenging. Therefore, horizontal and vertical variabilities of the fog layer also need ~~also~~ to be ~~much~~ more thoroughly explored in future field experiments. The horizontal variability especially at the onset of the fog also underlines that a point observation may not be very representative for what happens ~~in~~over a coarser grid box of a numerical weather prediction model~~ for instance~~.

One of the main points of this study is that fog water deposition ~~cannot~~should not be neglected ~~anymore~~ in 3D fog forecast models, as still often occurs. It ~~not only~~ influences not only microphysical fields near the ground but also the whole fog life cycle. It seem~~s~~ed to be more important than droplet sedimentation in our case, ~~keeping~~bearing in mind that ~~the concentration of small droplets was overestimated~~this observed case was characterized by small droplet concentrations and cloud mixing ratio. In this study, the deposition term ~~has been~~was introduced quite crudely and this would need some refinements in further studies. It would need to ~~be proportional to~~take account of the wind speed and the turbulence, and it could also consider the hygroscopic nature of canopies. By analogy with dry deposition, it would also be better to take ~~into account~~ droplet diameter into account, ~~supposing~~assuming that this field is correctly reproduced. Other studies have also shown that fog water deposition ~~wa~~is strongly enhanced at the forest edge, becoming up to 1.5-4 times larger than that in closed forest canopies (Katata, 2014), so it could be interesting to simulate the edge effect of fog water deposition. It is also crucial to perform measurements of fog water deposition and dewfall during field experiments (Price and Clark, 2014).

This study has shown the ~~strong~~great importance of some dynamical effects ~~which~~ operateing at ~~a~~ first order ~~to predict correctly~~for correct predictions of the fog life cycle. ~~But among all~~Despite the number of tests carried out, no~~-o~~ne ~~has~~ succeeded ~~to reproduce correctly~~in correctly reproducing the droplet concentration, which is always overestimated. Now that the fog life cycle ~~is~~has been correctly reproduced on this case, trying to correct this defect appears ~~as~~to be the main priority. Thouron et al. (2012) have developed a new scheme based on a supersaturation prognostic variable to avoid excessive droplet concentration in 2-moment microphysical schemes, as they have demonstrated that some assumptions of the adjustment process are no~~t~~ longer valid ~~anymore~~ with LES. One of the main points is ~~to take into account~~that the pre-existing cloud water should be taken into account as a sink of supersaturation, in order to limit the activation of cloud droplets. The relevance of this scheme, applied in Thouron et al. (2012) to cumulus and stratocumulus clouds, needs to be demonstrated for fog clouds, and this will be the subject of the second part of this study.

Acknowledgements. ~~A~~The authors are very grateful to all SIRTA operators and database managers. This research was partially funded by the European Community's Seventh Framework Programme (FP7/2007-2013) under the SESAR WP 11.2.2 project~~, under~~ (Grant Agreement 11-120809-C)

Name of ~~the~~ simulation	Difference of configuration with REF
NTR	No TRee: homogeneous surface
NDT	No Deposition on Trees
NDG	No Deposition (on Grass ~~and~~or trees)
DE~~5~~8	Deposition velocity equal to ~~5~~8 $\mathrm{cm\,s^{-1}}$
DX2	Horizontal resolution = 2m
WE3	3rd order WENO advection for momentum
WE5	5th order WENO advection for momentum
~~HM2~~	~~Initial RH minus 2%~~
~~HP3~~	~~Initial RH plus 3%~~
~~VM3~~	~~Geostrophic wind minus 3 $\mathrm{m\,s^{-1}}$~~
~~VP3~~	~~Geostrophic wind plus 3 $\mathrm{m\,s^{-1}}$~~

Table 1. Simulation configurations for sentivity tests

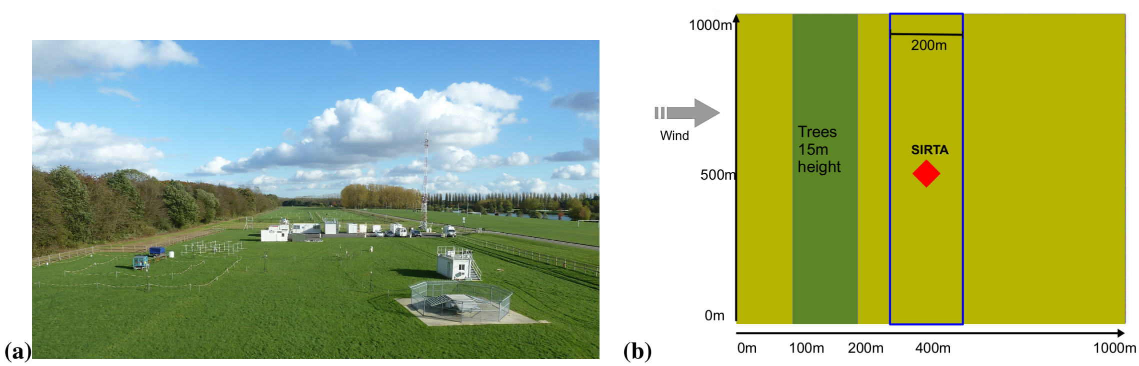

Figure 1. View of the measurement site (a) and modelling domain (b) with the tree~~s~~ barrier~~: a~~. All the simulated averaged results are presented ~~o~~in the blue contour area.

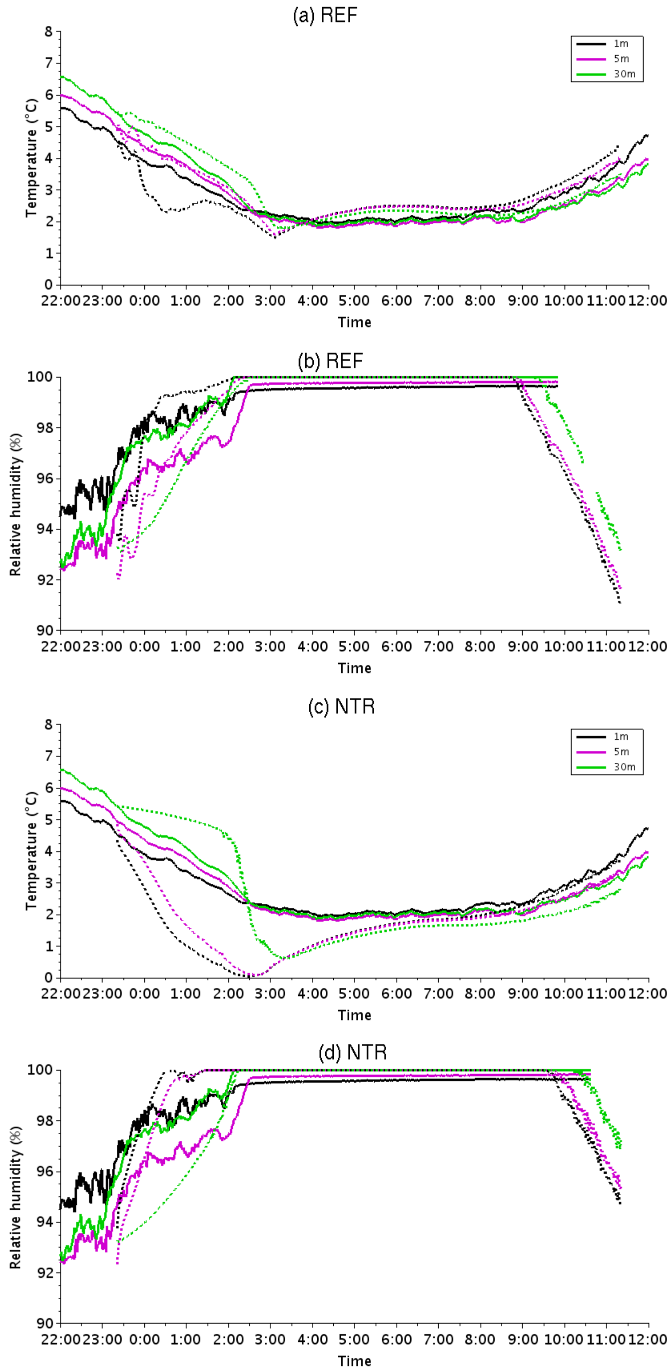

Figure 2. Observed (solid lines) and simulated (dashed lines) temporal evolution of temperature (a and c) and relative humidity (b and d) at 1m, ~~2m,~~ 5m~~, 10m, 20m~~ and 30m for the REF (a and b) and the NTR (without trees) (c and d) simulations. Simulated fields are averaged over the horizontal area located downstream of the tree barrier (blue contour area of Fig. 1b).

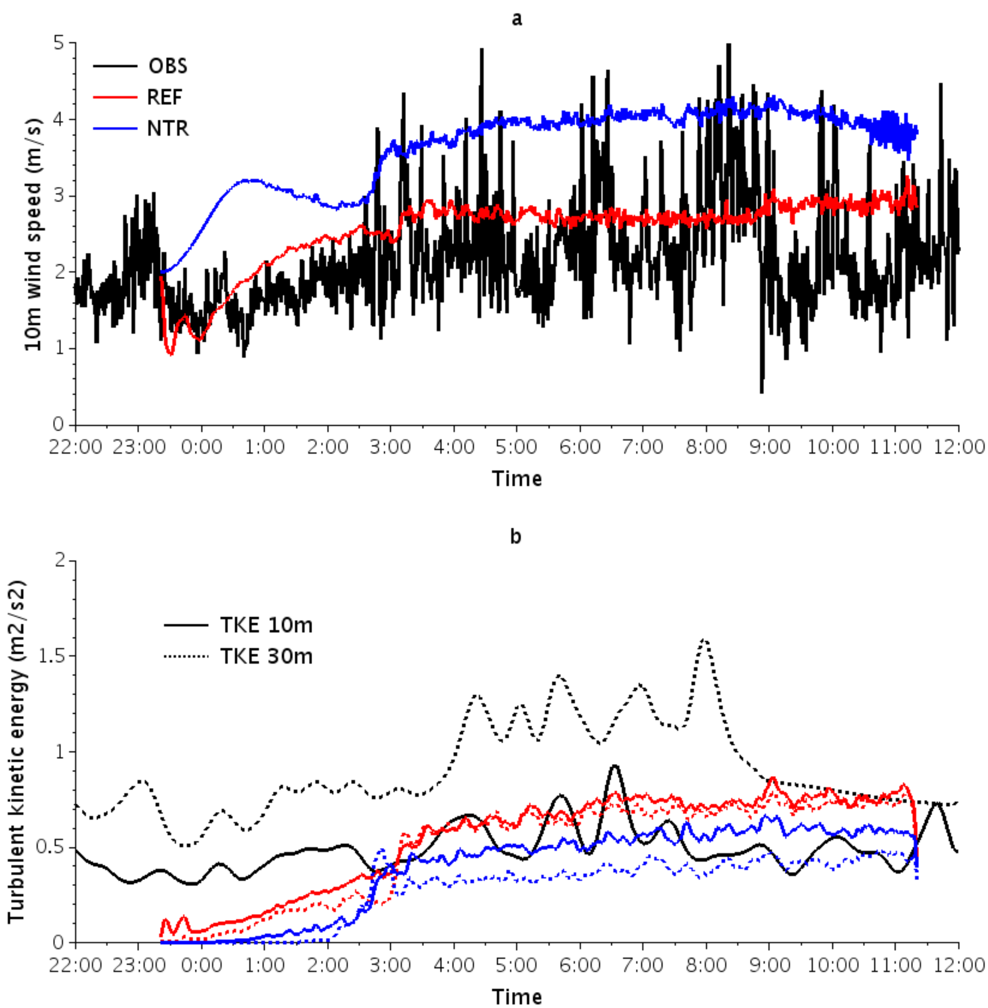

Figure 3. Observed (black lines) and simulated (~~color~~coloured lines) temporal evolution of 10m wind speed (a) and 10m (solid line) and 30m (dotted line) TKE (b) for the REF (red line) and the NTR (without trees) (blue line) simulations. Simulated fields are averaged over the horizontal area located downstream of the tree barrier (blue contour area of Fig. 1b).

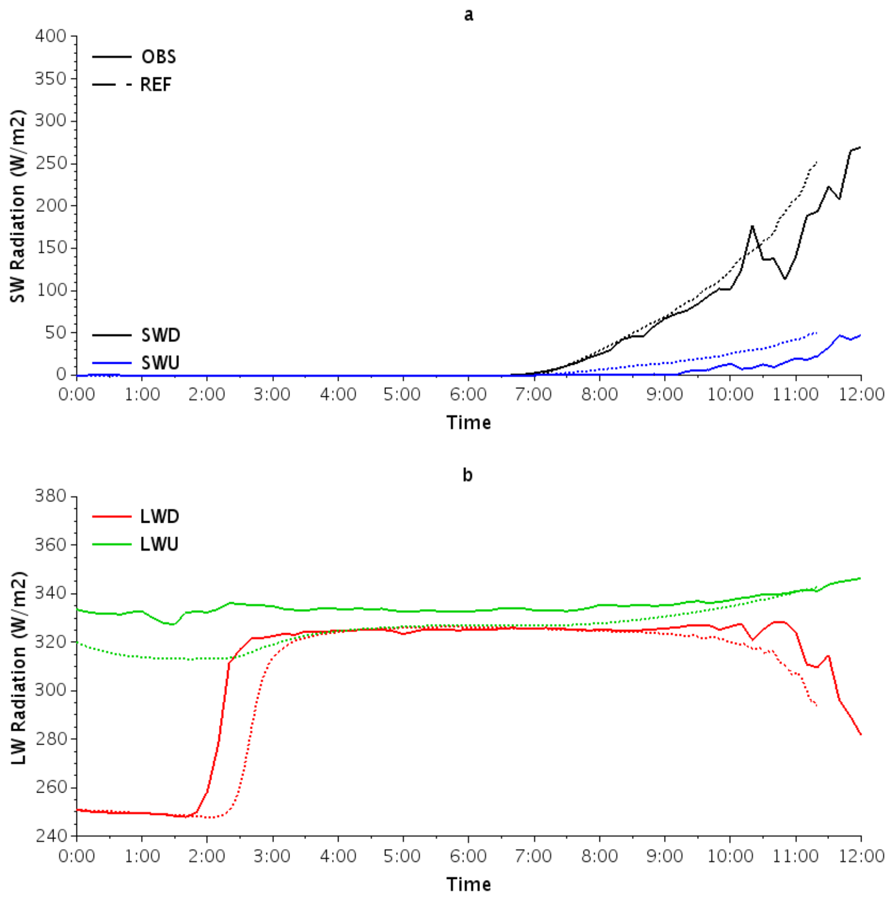

Figure 4. Observed (solid lines) and simulated (dotted lines, with the REF simulation) temporal evolution of downward and upward (at 1m) shortwave (a) and longwave (b) radiation fluxes (in W/m^2). Simulated fields are averaged over the horizontal area located downstream the tree barrier (blue contour area of Fig. 1b).

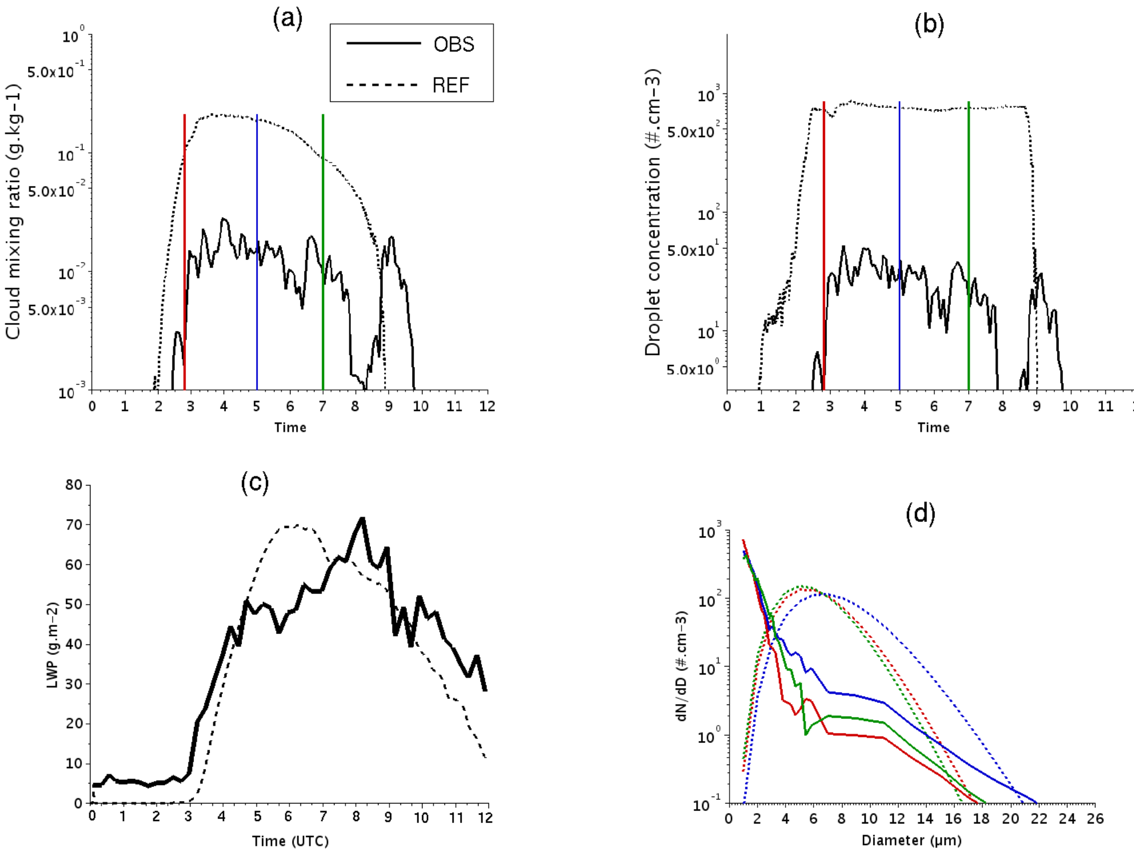

Figure 5. Time series of ~~droplet concentration (a, in cm^{-3}), liquid water content~~cloud mixing ratio (~~b~~a, in ~~g m^{3}~~g kg^{-1}), droplet concentration (b, in cm^{-3}),~~and~~ LWP (c, in g m^{-2}), and particle size distribution (d, in cm^{-3}) at 0250 UTC (in red), 0500 UTC (in blue) and 0700 UTC (in green) at 3 m agl observed (~~in~~ solid line), and simulated by REF (~~in~~ dotted line). Simulated fields are averaged over the horizontal area located downstream of the tree barrier (blue contour area of Fig. 1b).

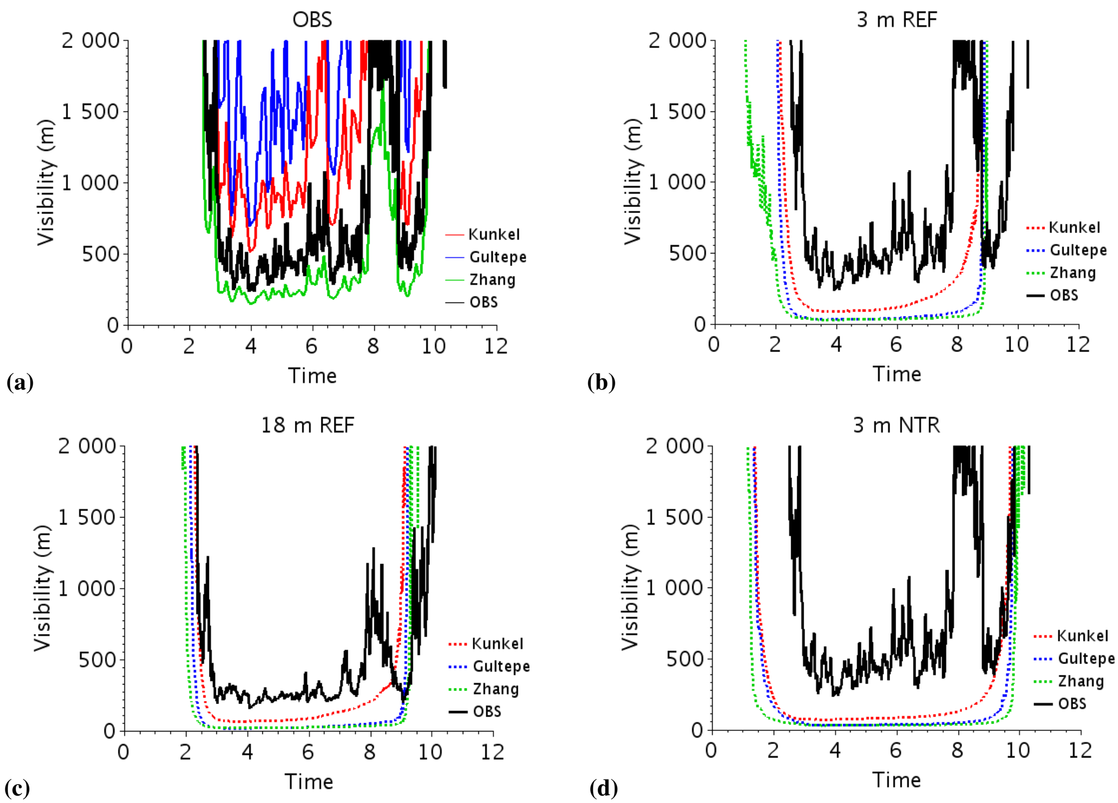

Figure 6. (a) 3 m observed (in black) and diagnosed (in colour) visibility with the observed microphysical fields according to Kunkel (1984), Gultepe et al. (2006) and Zhang et al. (2014a) (in m). (b) and (c) 3 m and 18m visibility diagnosed with the microphysical fields from the REF simulation. (d) 3 m visibility diagnosed with the microphysical fields from the NTR simulation (in m). Diagnosed visibility from simulations uses averaged microphysical fields over the horizontal area located downstream of the tree barrier (blue contour area of Fig. 1b).

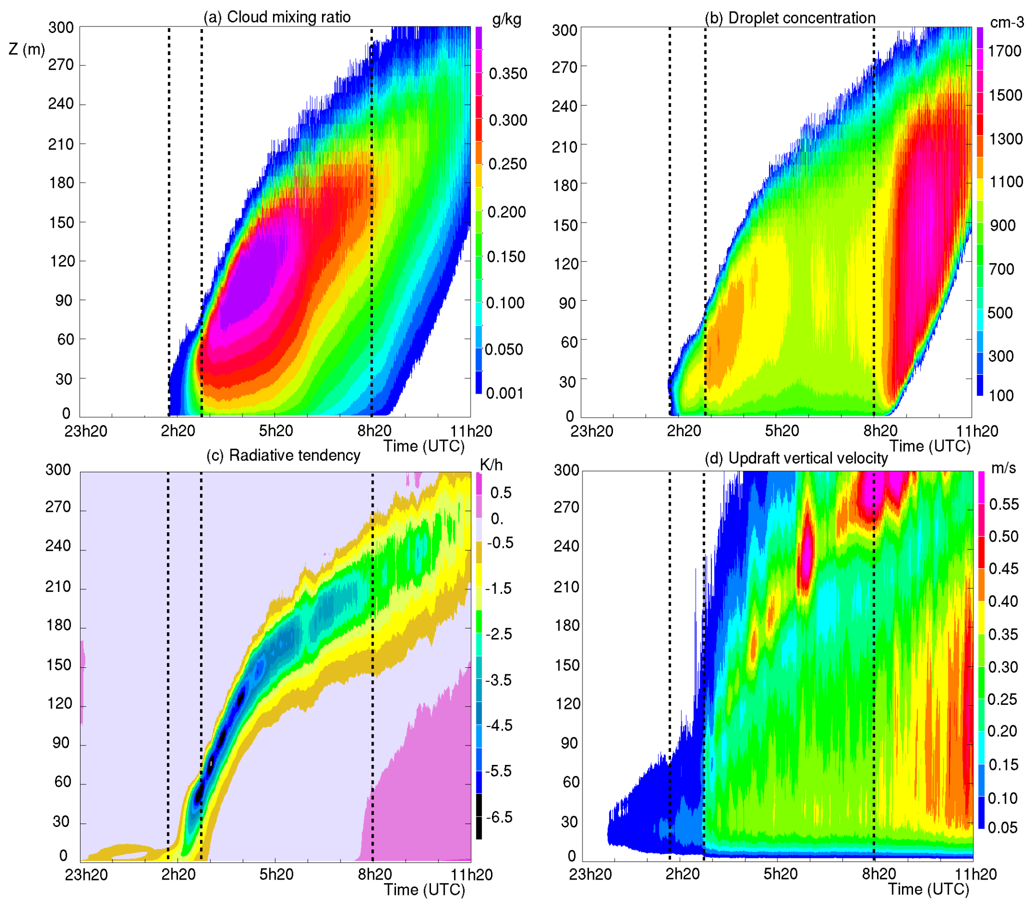

Figure 7. Temporal evolution of simulated vertical profiles of cloud mixing ratio (a, in $\mathrm{g\,kg^{-1}}$), droplet concentration (b, in $\mathrm{cm^{-3}}$), radiative tendency (c, in $\mathrm{K/h}$) and updraft vertical velocity (d, in $\mathrm{m\,s^{-1}}$) for the REF simulation. Fields are averaged over the horizontal area located downstream of the tree barrier (blue contour area of Fig. 1b). The three phases of the fog life cycle are delimited by dotted lines.

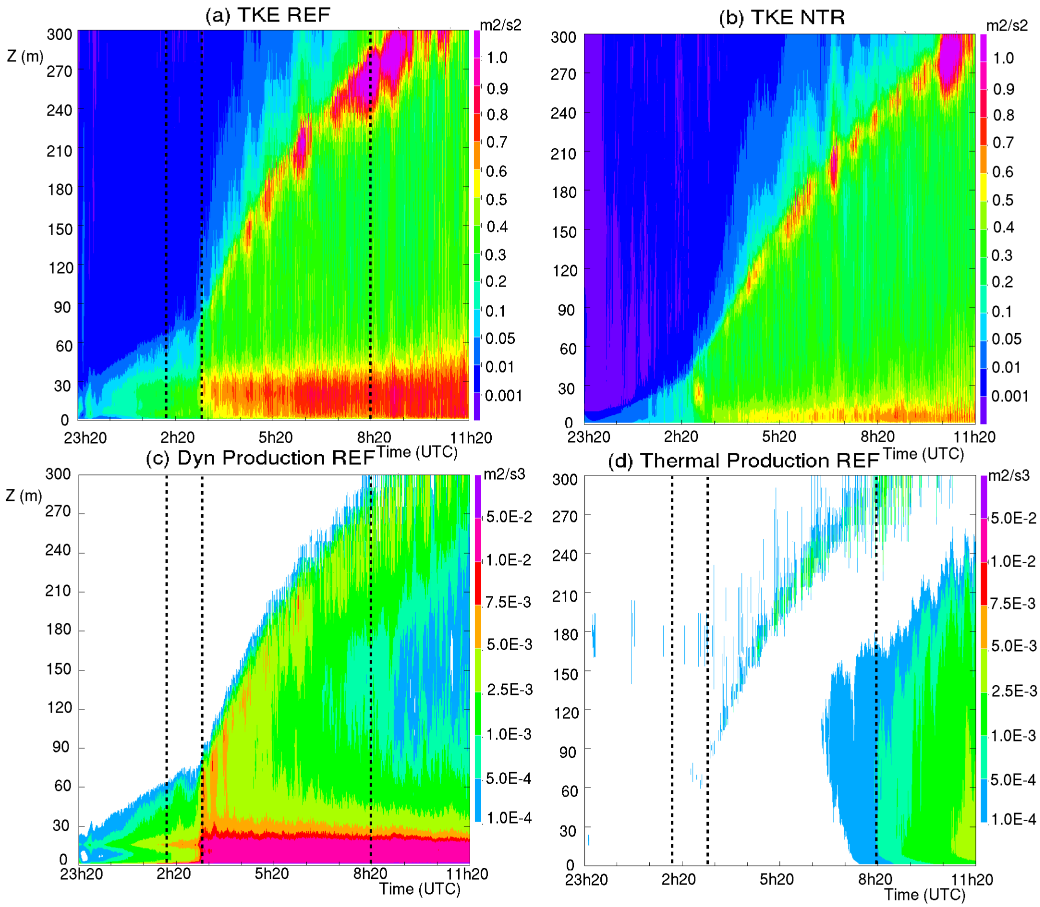

Figure 8. Temporal evolution of mean vertical profiles of total (resolved+subgrid) turbulent kinetic energy (in $m^2\,s^{-2}$) for REF (a) and NTR (b) simulations, and dynamical (c) and thermal (d) production of total turbulent kinetic energy (in $\mathrm{m}^2.\mathrm{s}^{-3}$) for the REF simulation. Fields are averaged over the horizontal area located downstream of the tree barrier (blue contour area of Fig. 1b). The three phases of the fog life cycle are delimited by dotted lines.

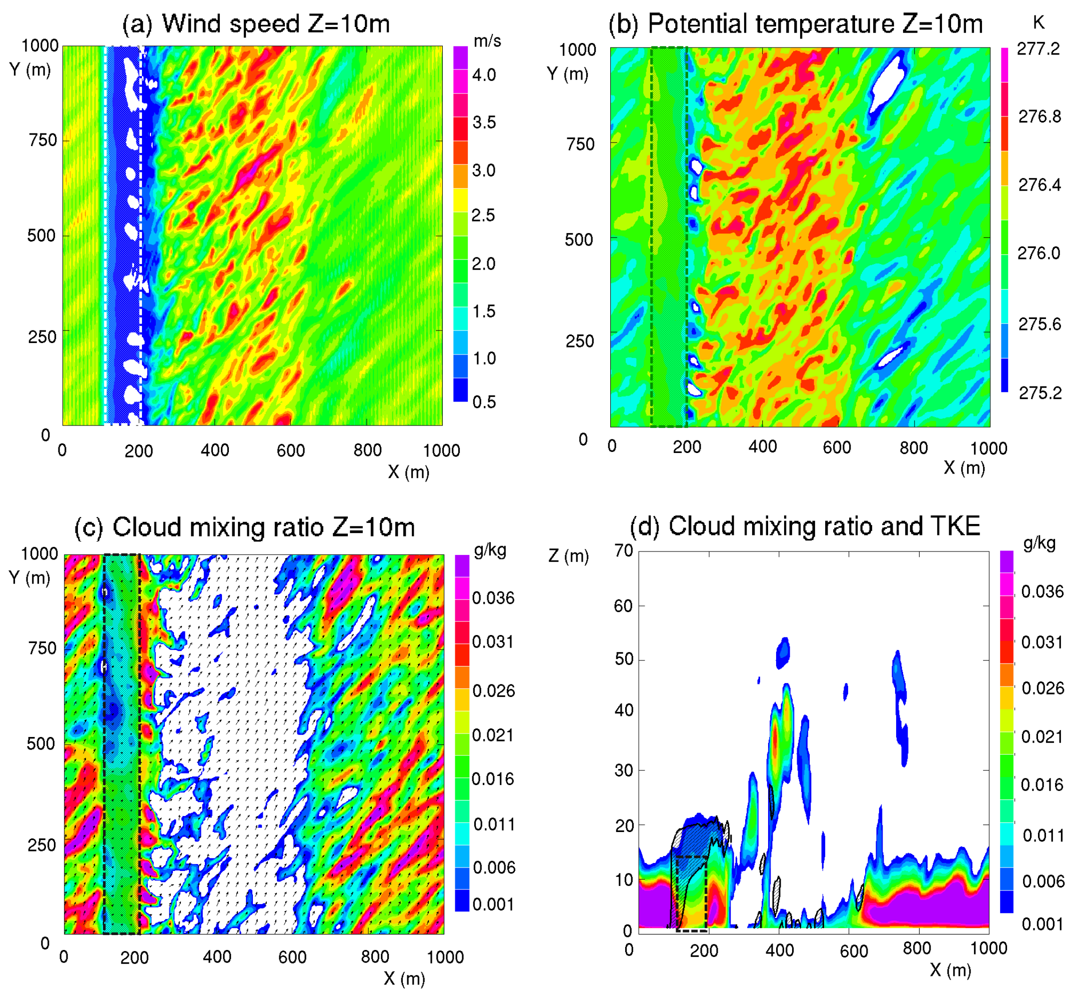

Figure 9. REF simulation at 02~~40~~10 UTC: (a), (b) and (c): Horizontal cross-section at 10 m height of wind speed (a, in $\mathrm{m\,s^{-1}}$), potential temperature (b, in K) and cloud mixing ratio (c, in $\mathrm{g\,kg^{-1}}$). (d): Vertical cross-section at Y=500m of cloud mixing ratio (in $\mathrm{g\,kg^{-1}}$) with area of TKE higher than $0.1\ \mathrm{m^2\,s^{-2}}$ shaded. The barrier of tree is marked with a rectangle.

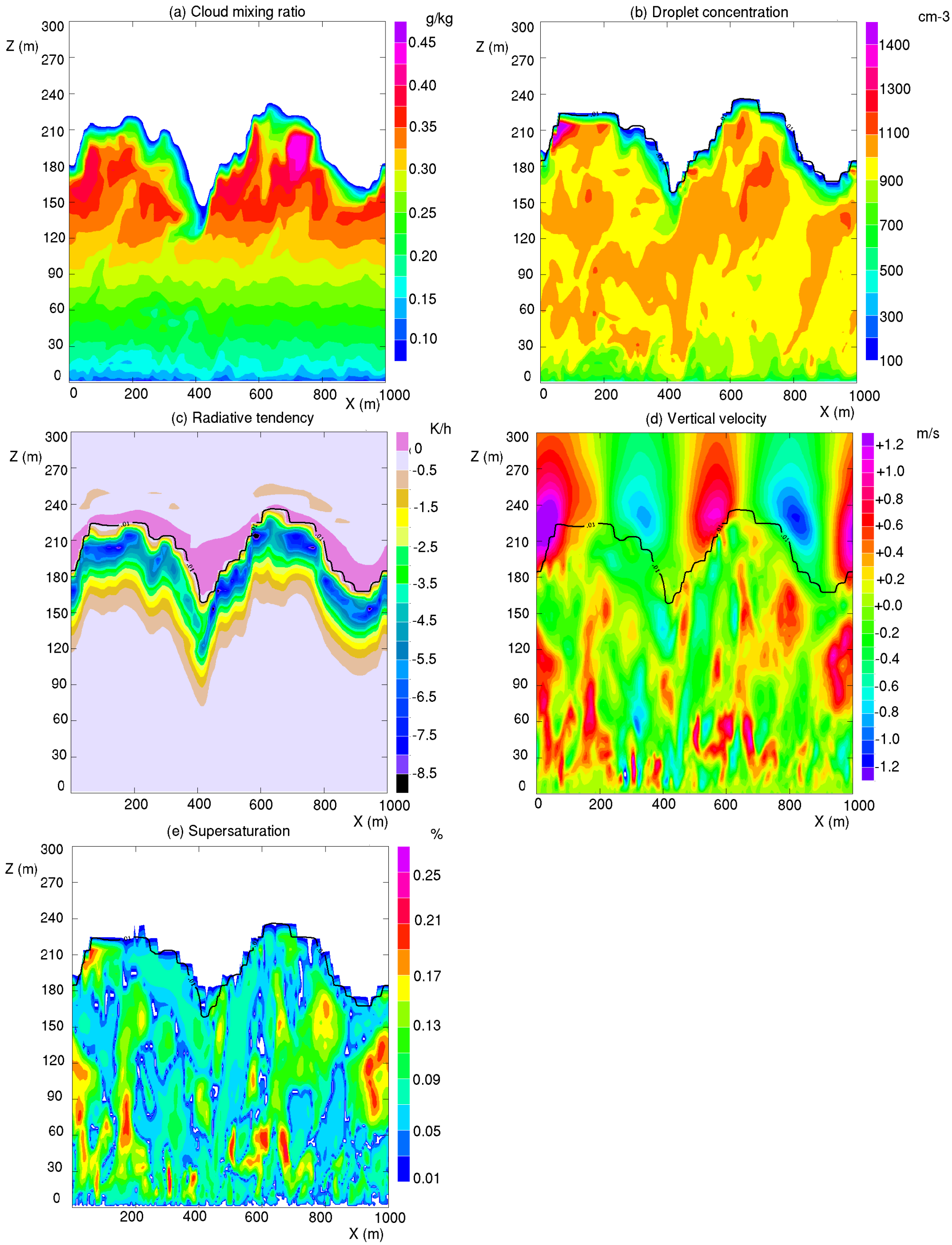

Figure 10. Vertical cross-section at Y=500m at 0620 UTC for the REF simulation: (a) cloud mixing ratio (in $\mathrm{g\,kg^{-1}}$), (b) droplet concentration (in $\mathrm{cm^{-3}}$), (c) radiative tendency (in $\mathrm{K/h}$), (d) vertical velocity (in $\mathrm{m\,s^{-1}}$) and (e) maximum of supersaturation (in $\%$) with the isoline of $r_c = 0.01\ \mathrm{g\,kg^{-1}}$ superimposed.

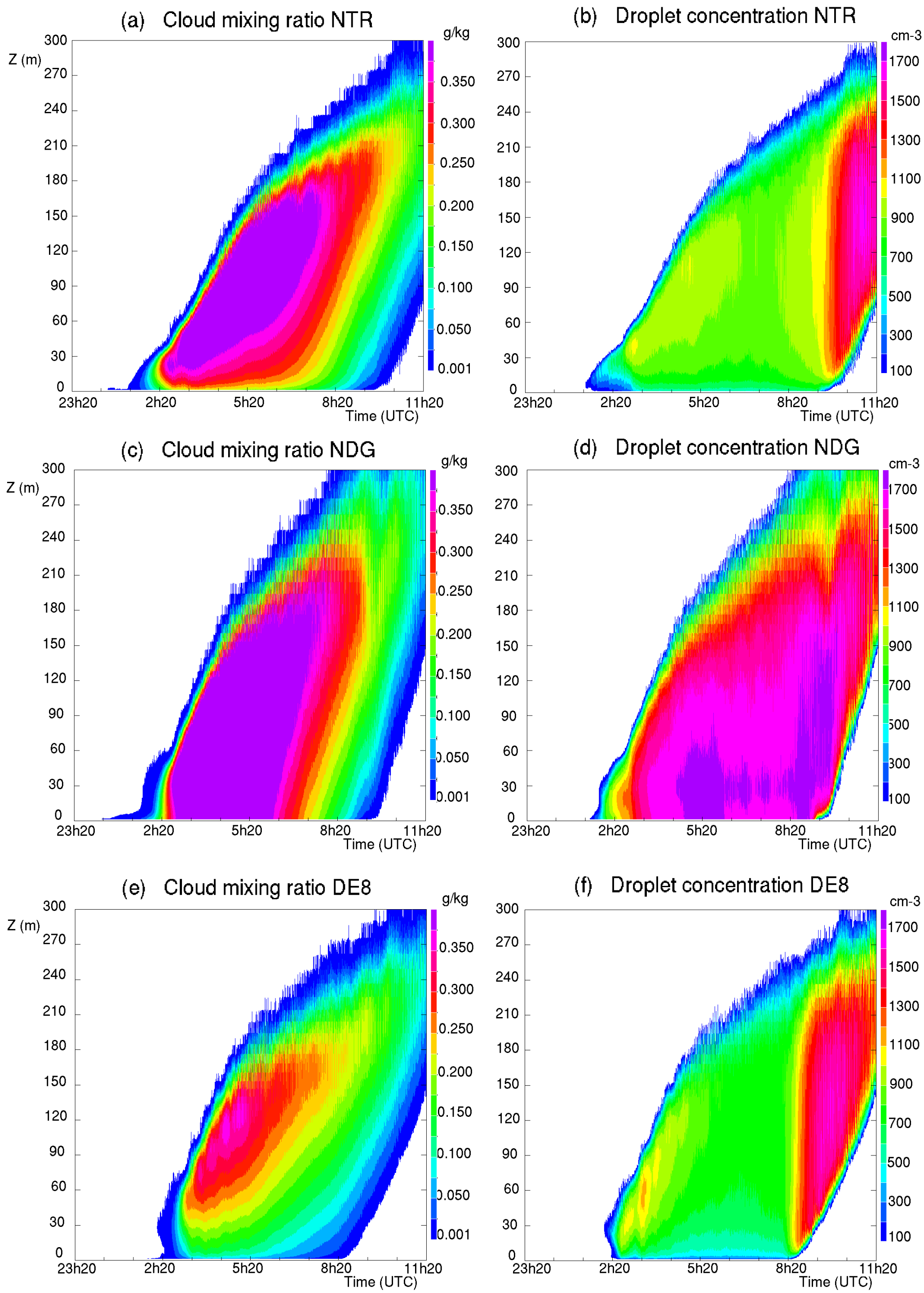

Figure 11. Temporal evolution of simulated vertical profiles of cloud mixing ratio (a, ~~and~~ c and e, in $\mathrm{g\,kg^{-1}}$) and droplet concentration (b, ~~and~~ d and f, in $\mathrm{cm^{-3}}$) for NTR~~and~~, NDG and DE8 simulations. Fields are averaged over the horizontal area located downstream of the tree barrier (blue contour area of Fig. 1b).

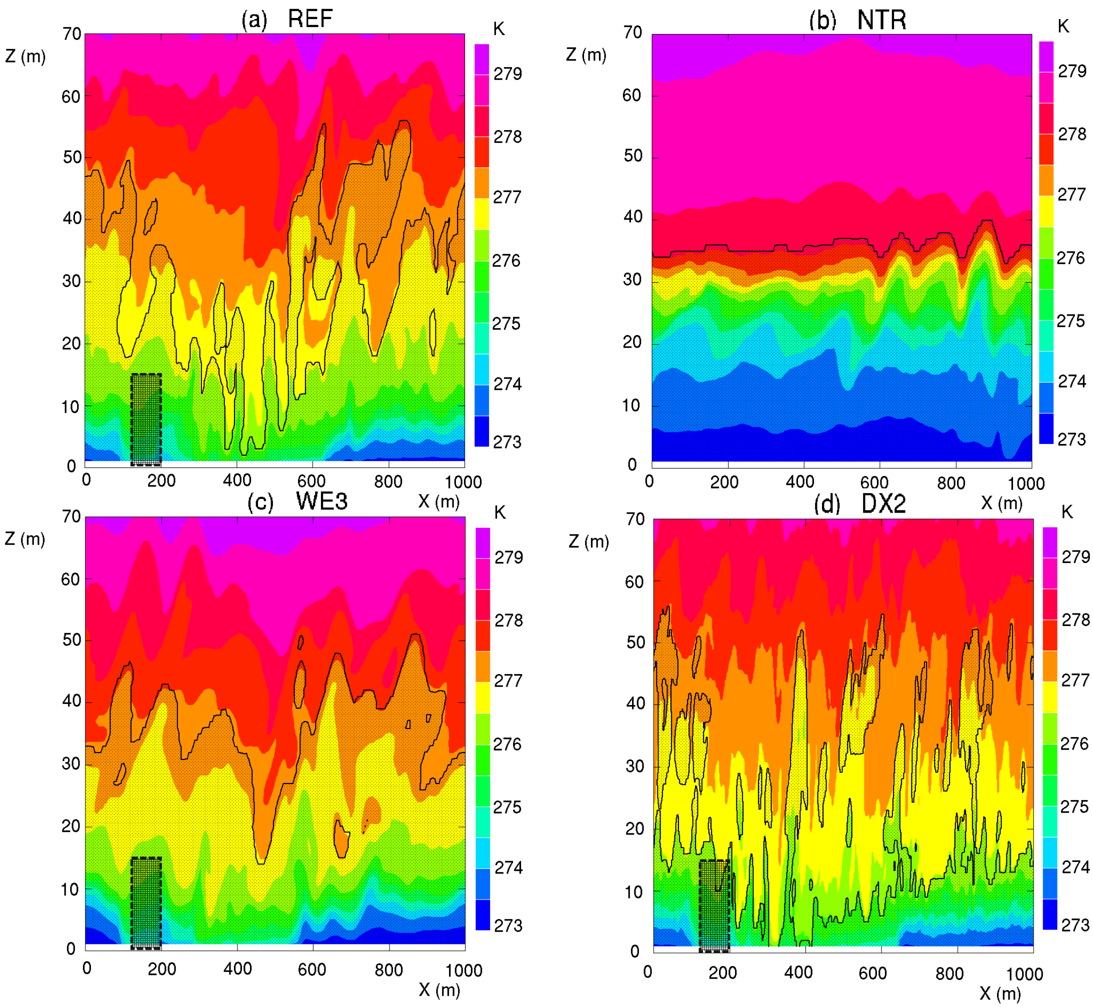

Figure 12. Vertical cross-sections at Y=500m and 0220 UTC of potential temperature (in K) for the REF (a), NTR (b), WE3 (c) and DX2 (d) simulations, with area of cloud mixing ratio higher than $0.1\,\mathrm{g\,kg^{-1}}$ superimposed with dots and the barrier of tree marked with a rectangle..

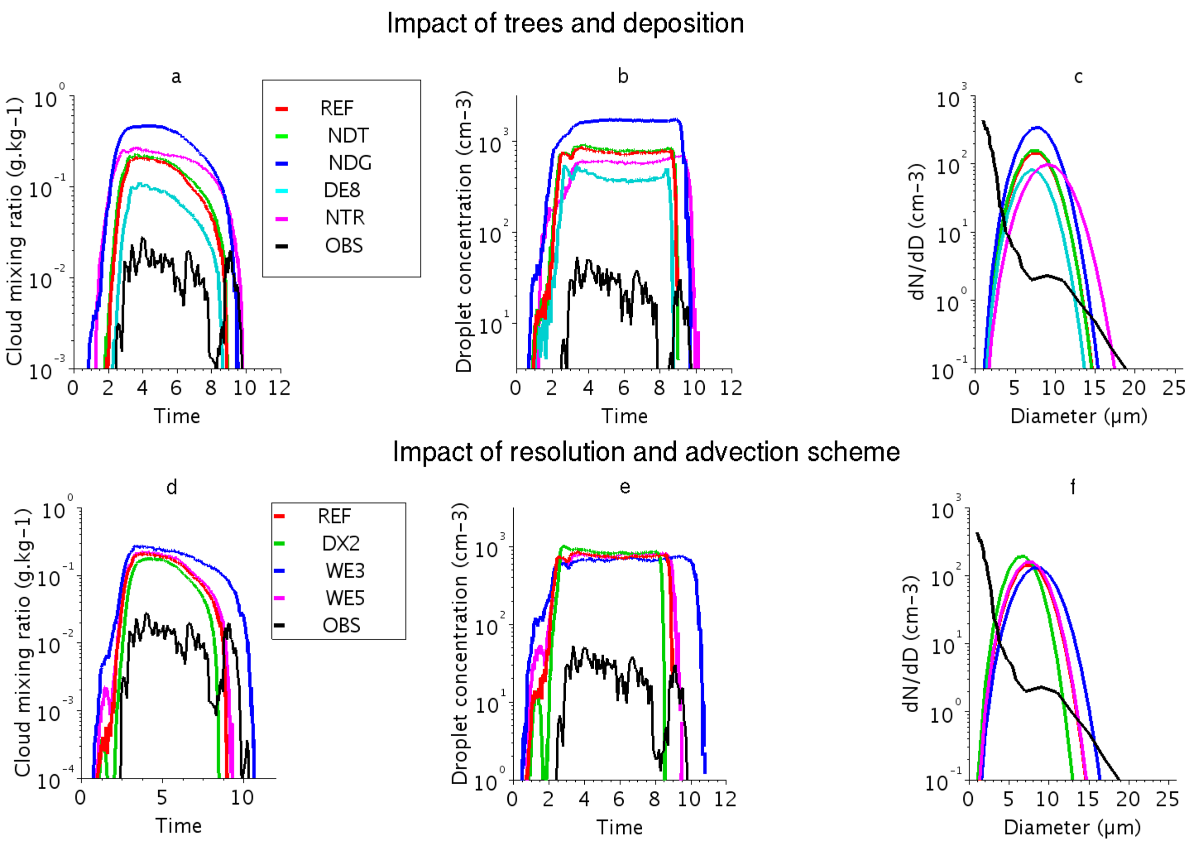

Figure 13. Time series of ~~droplet concentration (a, d and g, in cm^{-3}),~~ ~~liquid water content~~cloud mixing ratio (~~b, e and h~~a and d, in ~~g m^3~~g kg^{-1}), droplet concentration (b and e, in cm^{-3}), and droplet size distribution (~~e, f and i~~c nd f, in cm^{-3}) at 0520 UTC and 3 m agl observed (in black), and simulated (in colour). Simulated fields are averaged over the horizontal area located downstream of the tree barrier (blue contour area of Fig. 1b).

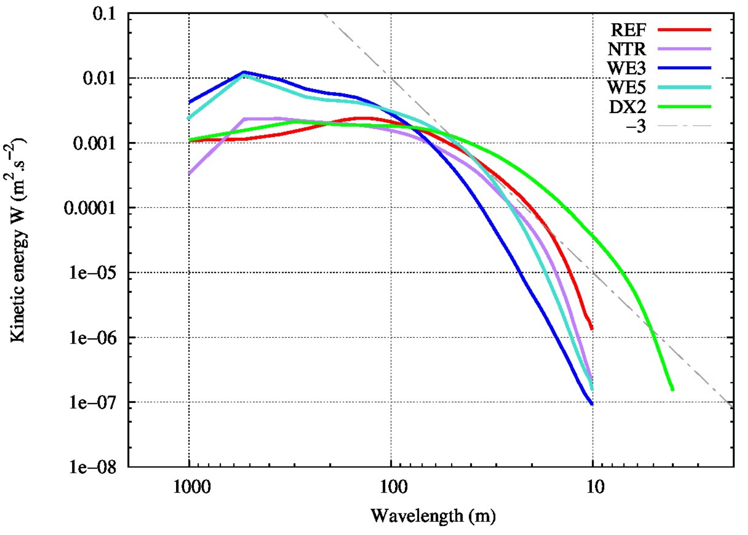

Figure 14. Mean kinetic energy spectra for vertical wind computed over the whole fog layer and horizontal domain at 0620 UTC for the REF, WE3, WE5, DX2 and NTR simulations.

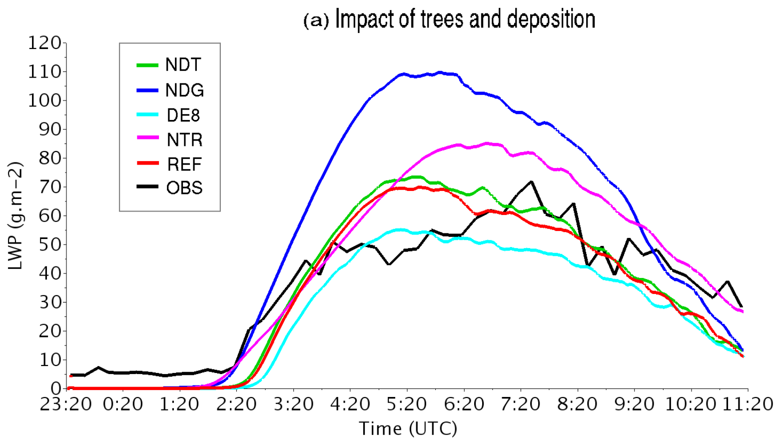

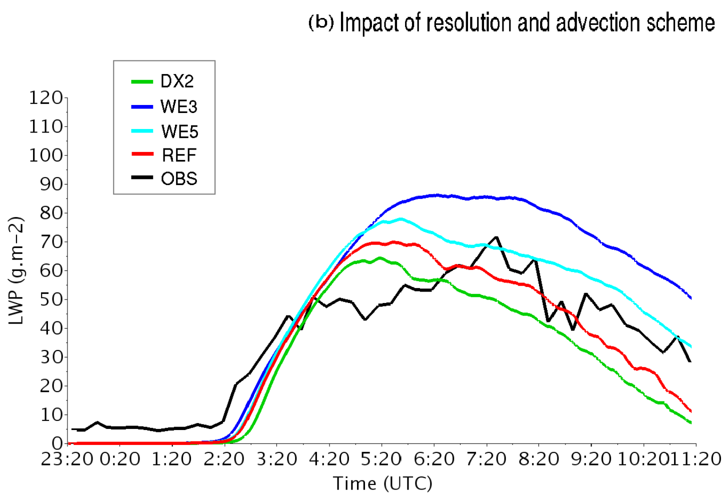

Figure 15. Time series of LWP (in $\mathrm{g\,m^{-2}}$) observed (in black), and simulated (in colour) for the different simulations. Simulated fields are averaged over the horizontal area located downstream of the tree barrier (blue contour area of Fig. 1b).

[A] Appendix: Material support

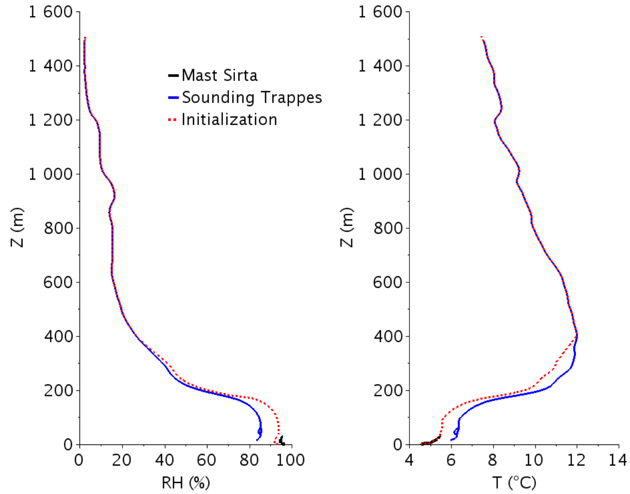

Figure A.1. Relative humidity (in $\%$) and temperature (in C) vertical profiles at 2320 UTC on 14 November 2011 observed at the Sirta mast (in black)~~,~~ and by the Trappes radiosounding (in blue) and used for the REF initialization.

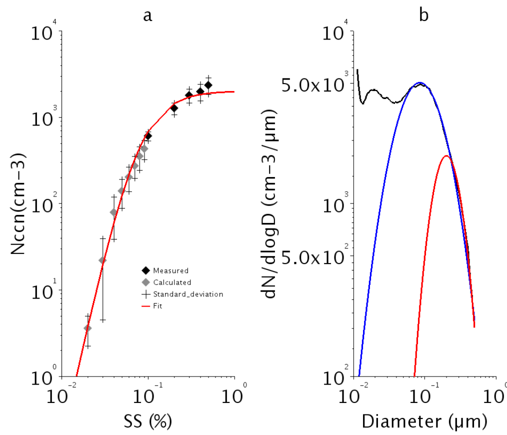

Figure A.2. (a) Activation spectrum: from CCNC measurement before the fog onset (between 0130 and 0230 UTC) for supersaturations higher than 0.1% in black dots, from calculation for supersaturations lower than 0.1% in grey dots, and fitted ~~from the~~using Cohard et al. (2000c)'s parametrization in red. (b) Particle size distribution from the aerosol measurements (in black), the lognormal distribution fitted on the accumulation mode (in blue) and according to Cohard et al. (2000c) (in red).

References

Aumond, P., V. Masson, C. Lac, B. Gauvreau, S. Dupont, and M. Berengier, 2013: Including the drag effects of canopies: real case large-eddy simulation studies. *Boundary-Layer Meteorology*, **146 (1)**, 65–80.

Baba, Y., and K. Takahashi, 2013: Weighted essentially non-oscillatory scheme for cloud edge problem. *Quarterly Journal of the Royal Meteorological Society*, **139 (674)**, 1374–1388.

Beare, R. J., and M. K. MacVean, 2004: Resolution sensitivity and scaling of large-eddy simulations of the stable boundary layer. *Boundary-Layer Meteorology*, **112 (2)**, 257–281.

Bergot, T., 2013: Small-scale structure of radiation fog: a large-eddy simulation study. *Quarterly Journal of the Royal Meteorological Society*, **139 (673)**, 1099–1112.

Bergot, T., 2015b: Large eddy simulation study of the dissipation of radiation fog. *Quarterly Journal of the Royal Meteorological Society*, **142**, 1029–1040.

Bergot, T., J. Escobar, and V. Masson, 2015a: Effect of small-scale surface heterogeneities and buildings on radiation fog: Large-eddy simulation study at Paris Charles de Gaulle airport. *Quarterly Journal of the Royal Meteorological Society*, **141 (686)**, 285–298.

Bergot, T., E. Terradellas, J. Cuxart, A. Mira, O. Liechti, M. Mueller, and N. W. Nielsen, 2007: Intercomparison of single-column numerical models for the prediction of radiation fog. *Journal of Applied Meteorology and Climatology*, **46 (4)**, 504–521.

Cohard, J.-M., J.-P. Pinty, and K. Suhre, 2000c: On the parameterization of activation spectra from cloud condensation nuclei microphysical properties. *Journal of Geophysical Research: Atmospheres (1984–2012)*, **105 (D9)**, 11 753–11 766.

Colella, P., and P. R. Woodward, 1984: The piecewise parabolic method (PPM) for gas-dynamical simulations. *Journal of Computational Physics*, **54 (1)**, 174–201.

Cuxart, J., P. Bougeault, and J.-L. Redelsperger, 2000: A turbulence scheme allowing for mesoscale and large-eddy simulations. *Quarterly Journal of the Royal Meteorological Society*, **126 (562)**, 1–30.

Deardorff, J. W., 1980: Stratocumulus-capped mixed layers derived from a three-dimensional model. *Boundary-Layer Meteorology*, **18 (4)**, 495–527.

Dupont, J.-C., M. Haeffelin, A. Protat, D. Bouniol, N. Boyouk, and Y. Morille, 2012: Stratus–fog formation and dissipation: a 6-day case study. *Boundary-layer meteorology*, **143 (1)**, 207–225.

Duynkerke, P. G., 1999: Turbulence, radiation and fog in Dutch stable boundary layers. *Boundary-Layer Meteorology*, **90 (3)**, 447–477.

Fouquart, Y., B. Bonnel, and V. Ramaswamy, 1991: Intercomparing shortwave radiation codes for climate studies. *Journal of Geophysical Research: Atmospheres*, **96 (D5)**, 8955–8968.

Fuzzi, S., and Coauthors, 1998: Overview of the Po valley fog experiment 1994 (CHEMDROP). *Contributions to Atmospheric Physics*, **71 (1)**, 3–19.

Geoffroy, O., J.-L. Brenguier, and I. Sandu, 2008: Relationship between drizzle rate, liquid water path and droplet concentration at the scale of a stratocumulus cloud system. *Atmospheric Chemistry and Physics*, **8 (16)**, 4641–4654.

Guedalia, D., and T. Bergot, 1994: Numerical forecasting of radiation fog. Part ii: A comparison of model simulation with several observed fog events. *Monthly Weather Review*, **122 (6)**, 1231–1246.

Gultepe, I., M. Müller, and Z. Boybeyi, 2006: A new visibility parameterization for warm-fog applications in numerical weather prediction models. *Journal of Applied Meteorology and Climatology*, **45 (11)**, 1469–1480.

Haeffelin, M., and Coauthors, 2010: PARISFOG: shedding new light on fog physical processes. *Bulletin of the American Meteorological Society*, **91 (6)**, 767–783.

Hammer, E., and Coauthors, 2014: Size-dependent particle activation properties in fog during the ParisFog 2012/13 field campaign. *Atmospheric Chemistry and Physics*, **14 (7)**, 10 517–10 533.

Katata, G., 2014: Fogwater deposition modeling for terrestrial ecosystems: A review of developments and measurements. *Journal of Geophysical Research: Atmospheres*, **119 (13)**, 8137–8159.

Khairoutdinov, M., and Y. Kogan, 2000: A new cloud physics parameterization in a large-eddy simulation model of marine stratocumulus. *Monthly Weather Review*, **128 (1)**, 229–243.

Koschmeider, H., 1924: Theorie der horizontalen sichtweite. beifs. *Phys. frei*, 33–53.

Kunkel, B. A., 1984: Parameterization of droplet terminal velocity and extinction coefficient in fog models. *Journal of Climate and Applied Meteorology*, **23 (1)**, 34–41.

Lafore, J., J. Stein, N. Asencio, P. Bougeault, V. Ducrocq, J. Duron, and C. Fischer, 1998: The Meso-NH atmospheric simulation system. Part i: Adiabatic formulation and control simulations. *Annales Geophysicae*, Vol. 16, 90–109.

Langlois, W., 1973: A rapidly convergent procedure for computing large-scale condensation in a dynamical weather model. *Tellus*, **25 (1)**, 86–87.

Lohnert, U., and S. Crewell, 2003: Accuracy of cloud liquid water path from ground-based microwave radiometry 1. dependency on cloud model statistics. *Radio Science*, **38 (3)**.

Lovett, G. M., J. J. Bowser, and E. S. Edgerton, 1997: Atmospheric deposition to watersheds in complex terrain. *Hydrological Processes*, **11 (7)**, 645–654.

Maalick, Z., T. Kuhn, H. Korhonen, H. Kokkola, A. Laaksonen, and S. Romakkaniemi, 2016: Effect of aerosol concentration and absorbing aerosol on the radiation fog life cycle. *Atmospheric Environment*, **133**, 26–33.

Masson, V., and Coauthors, 2013: The SURFEXv7. 2 land and ocean surface platform for coupled or offline simulation of earth surface variables and fluxes. *Geoscientific Model Development*, **6**, 929–960.

Mazoyer, M., F. Burnet, G. C. Roberts, M. Haeffelin, J.-C. Dupont, and T. Elias, 2016: Experimental study of the aerosol impact on fog microphysics. *Atmospheric Chemistry and Physics Discussions*, **2016**, 1–35.

Meyer, M. B., G. G. Lala, and J. E. Jiusto, 1986: Fog-82: A cooperative field study of radiation fog. *Bulletin of the American Meteorological Society*, **67 (7)**, 825–832.

Mlawer, E. J., S. J. Taubman, P. D. Brown, M. J. Iacono, and S. A. Clough, 1997: Radiative transfer for inhomogeneous atmospheres: RRTM, a validated correlated-k model for the longwave. *Journal of Geophysical Research: Atmospheres (1984–2012)*, **102 (D14)**, 16 663–16 682.

Morcrette, J.-J., 1991: Radiation and cloud radiative properties in the European Centre for Medium Range Weather Forecasts forecasting system. *Journal of Geophysical Research: Atmospheres*, **96 (D5)**, 9121–9132.

Nakanishi, M., 2000: Large-eddy simulation of radiation fog. *Boundary-Layer Meteorology*, **94 (3)**, 461–493.

Noilhan, J., and S. Planton, 1989: A simple parameterization of land surface processes for meteorological models. *Monthly Weather Review*, **117 (3)**, 536–549.

Porson, A., J. Price, A. Lock, and P. Clark, 2011: Radiation fog. Part ii: Large-eddy simulations in very stable conditions. *Boundary-Layer Meteorology*, **139 (2)**, 193–224.

Price, J., 2011: Radiation fog. Part i: observations of stability and drop size distributions. *Boundary-Layer Meteorology*, **139 (2)**, 167–191.

Price, J., and R. Clark, 2014: On the measurement of dewfall and fog-droplet deposition. *Boundary-Layer Meteorology*, **152 (3)**, 367–393.

Pruppacher, H. R., J. D. Klett, and P. K. Wang, 1998: Microphysics of clouds and precipitation.

Ricard, D., C. Lac, S. Riette, R. Legrand, and A. Mary, 2013: Kinetic energy spectra characteristics of two convection-permitting limited-area models AROME and Meso-NH. *Quarterly Journal of the Royal Meteorological Society*, **139 (674)**, 1327–1341.

Roach, W., R. Brown, S. Caughey, J. Garland, and C. Readings, 1976: The physics of radiation fog: I–a field study. *Quarterly Journal of the Royal Meteorological Society*, **102 (432)**, 313–333.

Roberts, G., and A. Nenes, 2005: A continuous-flow streamwise thermal-gradient ccn chamber for atmospheric measurements. *Aerosol Science and Technology*, **39 (3)**, 206–221.

Savijärvi, H., A. Arola, and P. Räisänen, 1997: Short-wave optical properties of precipitating water clouds. *Quarterly Journal of the Royal Meteorological Society*, **123 (540)**, 883–899.

Seity, Y., P. Brousseau, S. Malardel, G. Hello, P. Bénard, F. Bouttier, C. Lac, and V. Masson, 2011: The AROME-France convective-scale operational model. *Monthly Weather Review*, **139 (3)**, 976–991.

Shu, C.-W., 1998: Essentially non-oscillatory and weighted essentially non-oscillatory schemes for hyperbolic conservation laws. *Advanced numerical approximation of nonlinear hyperbolic equations*, Springer, 325–432.

Skamarock, W. C., 2004: Evaluating mesoscale nwp models using kinetic energy spectra. *Monthly Weather Review*, **132 (12)**, 3019–3032.

Slingo, A., 1989: A GCM parameterization for the shortwave radiative properties of water clouds. *Journal of the Atmospheric Sciences*, **46 (10)**, 1419–1427.

Stolaki, S., M. Haeffelin, C. Lac, J.-C. Dupont, T. Elias, and V. Masson, 2015: Influence of aerosols on the life cycle of a radiation fog event. A numerical and observational study. *Atmospheric Research*, **151**, 146–161.

Tardif, R., 2007: The impact of vertical resolution in the explicit numerical forecasting of radiation fog: A case study. *Pure and Applied Geophysics*, **164 (6-7)**, 1221–1240.

Thouron, O., J.-L. Brenguier, and F. Burnet, 2012: Supersaturation calculation in large eddy simulation models for prediction of the droplet number concentration. *Geoscientific Model Development*, **5 (3)**, 761–772.

Uematsu, A., M. K. Yamamoto, H. Hashiguchi, K. Hirashima, and S. Fukao, 2005: Shear-induced roll structure of fog observed by a millimeter-wave scanning Doppler radar. *Geophysical Research Letters*, **32 (14)**.

von Glasow, R., and A. Bott, 1999: Interaction of radiation fog with tall vegetation. *Atmospheric Environment*, **33 (9)**, 1333–1346.

Wendisch, M., and Coauthors, 1998: Drop size distribution and LWC in Po valley fog. *Contributions to Atmospheric Physics*, **71 (1)**, 87–100.

Ye, X., B. Wu, and H. Zhang, 2015: The turbulent structure and transport in fog layers observed over the Tianjin area. *Atmospheric Research*, **153**, 217–234.

Zaïdi, H., E. Dupont, M. Milliez, L. Musson-Genon, and B. Carissimo, 2013: Numerical simulations of the microscale heterogeneities of turbulence observed on a complex site. *Boundary-Layer Meteorology*, **147 (2)**, 237–259.

Zhang, J., H. Xue, Z. Deng, N. Ma, C. Zhao, and Q. Zhang, 2014a: A comparison of the parameterization schemes of fog visibility using the in-situ measurements in the North China Plain. *Atmospheric Environment*, **92**, 44–50.

Zhang, X., L. Musson-Genon, E. Dupont, M. Milliez, and B. Carissimo, 2014b: On the influence of a simple microphysics parametrization on radiation fog modelling: A case study during ParisFog. *Boundary-Layer Meteorology*, **151 (2)**, 293–315.